Macromolecular crowding meets tissue engineering by self-assembly: A paradigm shift in regenerative medicine

*Abhigyan Satyam, Pramod Kumar, Xingliang Fan, Alexander Gorelov, Yury Rochev, Lokesh Joshi, Héctor Peinado, David Lyden, Benjamin Thomas, Brian Rodriguez, Michael Raghunath, Abhay Pandit and Dimitrios Zeugolis**

Mr. A. Satyam, Mr. P. Kumar, Mr. X. Fan, Dr. Y. Rochev, Prof. A. Pandit, Dr. D. Zeugolis
Network of Excellence for Functional Biomaterials (NFB), National University of Ireland Galway, (NUI Galway), Galway, Ireland
E-mail: dimitrios.zeugolis@nuigalway.ie

Dr. A. Gorelov
School of Chemistry, University College Dublin, Dublin, Ireland

Prof. L. Joshi
Alimentary Glycoscience Research Cluster, NUI Galway, Galway, Ireland

Dr. H. Peinado, Prof. D. Lyden
Children's Cancer and Blood Foundation Laboratories, Departments of Pediatrics, Cell and Developmental Biology, Weill Cornell Medical College, New York, USA

Dr. B. Thomas
Sir William Dunn Pathology School, Oxford University, Oxford, UK

Dr. B. Rodriguez
Institute of Biomolecular & Biomedical Research, University College Dublin, Dublin, Ireland

Prof. M. Raghunath
Tissue Modulation Laboratory, National University of Singapore, Singapore

Keywords: macromolecular crowding, macromolecular polydispersity, excluding volume effect, extracellular matrix deposition, cell-sheet tissue engineering

Advancements in molecular and cell biology have led to the development of cell-based therapies to treat injured or degenerated tissues.[1] The rationale of this concept is that functional regeneration can be achieved best by using the innate capacity of cells to create their own tissue-specific extracellular matrix (ECM) avoiding the shortfalls of man-made devices. Although direct cell injections have demonstrated very promising preclinical and clinical outcomes,[2] the mode of administration offers little control over local retention and distribution of the injected cell suspensions[3] leading to scattered therapeutic efficiency. This deficiency has led to the development of living substitutes for skin[4] and blood vessel[5] composed of cells seeded on a collagen scaffold. Notwithstanding the efficacious results in preclinical models and clinical trials, it soon became apparent that the presence of the scaffold hinders tissue remodelling and function.[6] These drawbacks led to the development of the scaffold-free cell-sheet tissue engineering (CSTE)[7] or tissue engineering by self-assembly (TESA),[8] a therapy that offers the fabrication of a contiguous cell sheet that is stabilised by cell-cell contacts and endogenously produced ECM. Despite the documented, in preclinical and clinical setting, positive outcomes for skin,[9] blood vessel,[10, 11] cornea,[12, 13] heart,[14] lung,[15] liver[16] and bone[17] replacement, only Epicel® (Genzyme, USA) for skin and LifeLine™ for blood vessel (Cytograft, USA) have been commercialised so far. This limited technology transfer from bench-top to clinic has been attributed to the substantial long period of time required for *ex vivo* culture (e.g. 14-35 days for corneal epithelium;[13] 84 days for corneal stromal;[18] 28 days for corneal endothelium;[19] 70 days for lung cell-sheet;[15] and 196 days for blood vessel[11]) that often leads to loss of native phenotype and cell senescence.[20]

Here, we propose a biophysical approach, termed macromolecular crowding (MMC), that increases thermodynamic activities and biological processes by several orders of magnitude,[21] as means to create ECM-rich tissue equivalents. The principle of MMC is derived from the notion that *in vivo* cells reside in a highly crowded/dense extracellular space and therefore the conversion of the *de novo* synthesised procollagen to collagen I is rapid.[22] However, in the even substantially more dilute than body fluids (e.g. urine: 36-50g/l; blood: 80g/l) culture conditions (e.g. HAM F10 nutrient medium: 16.55g/l; DMEM/F12 medium: 16.78g/l; DMEM high glucose and L-glutamine medium: 17.22g/l), the rate limiting conversion of procollagen to collagen I is very slow (**Figure 1a**). We propose that the

addition of inert polydispersed macromolecules (presented as spherical objects of variable diameter in **Figure 1b**) in the culture media will facilitate amplified production of ECM-rich living substitutes.

To acquire maximum ECM deposition under MMC conditions from human fibroblasts, optimal culture period, serum origin and serum concentration were assessed. Sodium dodecyl sulphate polyacrylamide gel electrophoresis (SDS-PAGE; **Supplementary Figure S1**) and complementary densitometric analysis (**Figure 2a**) revealed that the maximum (p<0.0001) collagen type I deposition was achieved after culturing WI38 human lung fibroblasts for 2 days at 0.5% foetal bovine serum (FBS) in the presence of 100μg/ml 500kDa dextran sulphate (DxS). In fact, an almost 30-fold increase in collagen deposition was observed in comparison to the non-MMC control counterparts. The reduction in collagen content as a function of increased FBS concentration and time in culture was attributed to the inherently high matrix metalloproteinase-2 (MMP-2) content of FBS, as revealed by gelatin zymography (**Figure 2b** and **Supplementary Figure S2**). Immunocytochemistry (ICC) analysis corroborated the high collagen type I deposition at low FBS concentrations and also confirmed the fibrillar pattern of collagen and fibronectin (**Figure 2c**). Similar results were obtained in WS1 human skin fibroblast culture under MMC conditions (100μg/ml 500kDa DxS at 0.5% FBS after 2, 4 and 6 days in culture), as revealed by SDS-PAGE and complementary densitometric analysis (**Supplementary Figure S3**), gelatin zymography (**Supplementary Figure S4**) and ICC analysis (**Supplementary Figure S5**). In this case, an almost 70-fold increase in collagen deposition was observed, in comparison to the non-MMC control counterparts. Phase contrast microscopy (results not shown) revealed that WI38 and WS1 fibroblasts maintained their spindle-shaped morphology independent of the presence of DxS, FBS concentration (0-10%) for all time points (2, 4 and 6 days).

To avoid xenogeneic contaminants, the influence of human serum (HS), as an alternative to FBS, was assessed. MMC (100μg/ml 500kDa DxS) resulted in a 30- and 80-fold increase in collagen deposition for the WI38 and the WS1 fibroblasts respectively after 2 days in culture using 0.5% HS (**Supplementary Figure S6** and **S7** respectively); a reduction in collagen content as a function of increased HS concentration and time in culture due to the inherently

high MMP-2 content of HS (**Supplementary Figure S2** and **S8**); and maintenance of physiological cell morphology (results not shown).

Having identified the 0.5% HS as the optimal serum concentration and 2 days as the optimal culture time for maximum ECM deposition in the presence of 100μg/ml 500kDa DxS, we ventured to identify the optimal macromolecular crowder for maximum ECM deposition. It was hypothesised that molecular polydispersity is the key modulator of excluding volume, and its complement available volume, and therefore polydispersed macromolecules will induce maximum ECM deposition. Dynamic light scattering (DLS) analysis of neutral (Ficoll™70, Ficoll™400 and combination of thereof) and negatively (DxS 500kDa and carrageenan, CR) charged macromolecules revealed that CR has the highest hydrodynamic diameter (**Supplementary Figure S9**), whist high-resolution particle size distribution, using Nanoparticle Tracking Analysis (NTA), demonstrated that CR has the highest polydispersity (**Figure 3a**).

SDS-PAGE (**Supplementary Figure S10a**), densitometry (**Supplementary Figure S10b**) and phase contrast microscopy (results not shown) identified the 75μg/ml as the optimal CR concentration. Subsequent culture of WI38 and WS1 fibroblasts with 0.5% FBS and HS with variable dispersity macromolecules and subsequent SDS-PAGE (**Supplementary Figure S11**), densitometry (**Figure 3b**) and ICC (**Figure 3c**) analysis validated our hypothesis that maximum ECM deposition can be achieved by the most polydispersed macromolecule, distinguishing CR as the most suitable molecule. Phase contrast microscopy revealed that WI-38 and WS-1 fibroblasts (results not shown) maintained their spindle-shaped morphology independent of the crowder species used. alamarBlue® (**Supplementary Figure S12**) and Live/Dead® (**Supplementary Figure S13**) analysis demonstrated that MMC did not affect cell metabolic activity and viability, respectively.

After optimisation of MMC culture condition, ECM-rich cell-assembled constructs were produced and characterised. Due to the abundance in ECM deposition in the presence of 0.5%

HS and 75μg/ml CR, traditional thermo-responsive N-isopropyl acrylamide (pNIPAAm) coating alone was not suitable for the detachment of intact ECM-rich WS-1 fibroblasts sheets, even only after 2 days in culture (**Figure 4a**). A 65% N-isopropyl acrylamide / 35% N-tert-butyl acrylamide (pNIPAAm + pNTBA) copolymer allowed for very first time attachment (**Figure 4b**) and detachment (**Figure 4c**) of intact ECM-rich WS-1 fibroblast sheets, produced after 2 days in the presence of 0.5% HS and 75μg/ml CR. Further time-lapse microscopy indicates that the detachment rate of the WS-1 fibroblasts sheets under MMC conditions (0.5% HS and 75μg/ml CR, 2 days in culture; **Supplementary Figure S14a-c, g**) was slower than their non-MMC counterparts (**Supplementary Figure S14d-f, g**), due to the abundance in deposited ECM. ICC (**Figure 4d-k**), Masson's Trichrome (**Supplementary Figure S15**), Picro Sirius red (**Figure 4l, o**) and scanning electron microscopy (**Figure 4m, p**) analysis further corroborate the enhanced ECM deposition, the fibrillar pattern and tissue like organisation of cell-sheets produced under MMC crowding conditions (0.5% HS and 75μg/ml CR) within 2 days of culture. Atomic force microscopy (**Figure 4n, q; Supplementary Figure S16**) revealed the presence of significantly more fibrous structure in the intercellular regions on the cell sheet surface under MMC crowding conditions, consistent with the presence of collagen. The fibrous ECM (**Supplementary Figure S17**) was visible also under no MMC crowding conditions.

To assess the influence of MMC (0.5% HS and 75μg/ml CR, 2 days in culture) on molecular functions, cellular components and biological processes proteomics analysis (**Supplementary Table. 1, 2a and 2b**) was carried out, which was subsequently validated with ICC (**Figure. 5a; Supplementary Figure S18a**) and complementary fluorescence intensity **(Figure 5b; Supplementary Figure S18b)** measurements. Data obtained confirmed significant upregulation (p<0.0001) of collagenous proteins (e.g. collagen type I, III, IV, V, and VI); enzymes associated with biogenesis of connective tissue proteins and cross-linking of collagen and elastin (e.g. lysyl oxidase); basement membrane proteins (e.g. laminin);

glycoproteins (e.g. fibronectin); glycosaminoglycans (e.g. hyaluronic acid); and proteoglycans (e.g. decorin). Other ECM proteins (e.g. collagen type VII, elastin, fibrillin-1); enzymes associated with collagen maturation and cross-linking (e.g. transglutaminase-2); cytoskeletal proteins (e.g. α-smooth muscle actin, epithelial keratin, tubulin); glycosaminoglycans (e.g. chondroitin sulphate, keratin sulphate, heparin sulphate); proteoglycans (e.g. aggrecan, biglycan); and cytokines (e.g. TEM-1/CD248, IL-10) remained unaffected (**Supplementary Figure S18**), indicating that MMC does not impair physiological function.

The high ECM deposition procedure can be readily applied to other cell types, irrespective of the amounts of ECM secreted. Here, we generated cohesive tissue modules from human tenocytes and osteoblasts (**Figure 6**). SDS-PAGE (**Supplementary Figure S19**) and complementary densitometric analysis (**Figure 6a**) revealed that the maximum (p<0.0001) collagen type I deposition was achieved after culturing human tenocytes for 6 days at 5% FBS in the presence of 75μg/ml CR. In fact, an almost 15-fold increase in collagen type I deposition was observed in comparison to the non-MMC control counterparts. ICC analysis corroborated the high deposition of collagenous proteins (collagen type I, III, IV, V and VI), glycoproteins (e.g. fibronectin) and basement membrane proteins (e.g. laminin), whilst tenomodulin expression remained unaffected (**Figure 6b**). Analogous was the situation with human osteoblasts. Specifically, SDS-PAGE (**Supplementary Figure S20**) and complementary densitometric analysis (**Figure 6c**) revealed that the maximum (p<0.0001) collagen type I deposition was achieved after culturing human osteoblasts for 4 days at 5% FBS in the presence of 75μg/ml CR. In fact, an almost 20-fold increase in collagen type I deposition was observed in comparison to the non-MMC control counterparts. ICC analysis corroborated the high deposition of collagenous proteins (e.g. collagen type I, III, IV, V and VI), glycoproteins (e.g. fibronectin) and basement membrane proteins (e.g. laminin), whilst tenomodulin expression remained unaffected (**Figure 6d**). alamarBlue® and Live/Dead®

analysis (results not shown) demonstrated that CR did not affect tenocyte and osteoblast metabolic activity.

CSTE / TESA therapies utilise the inherent capacity of cells to create three-dimensional tissue-specific equivalents, bypassing the drawbacks associated with biodegradable scaffolds.[23] Moreover, the presence of cell-produced ECM, through secretion of paracrine and proliferative signals, minimises cell apoptosis, thus improving vascularisation and facilitating tight adherence onto the host tissues.[24] Despite the significant strides that have been made to-date, scaffold-less regeneration approaches require prolonged *ex vivo* culture (14 to 196 days), which impedes clinical translation and commercialisation of such technologies. Moreover, the far from physiological culture systems fail to emulate native tissue microenvironment, resulting in cellular senescence, phenotypic drift, growth arrest and loss of stem cell multipotency, even after a few hours in culture.[25]

Here, we utilised the potential of MMC, a biophysical phenomenon with energetic consequences in biological processes,[26] to create within 48 hours and at 0.5% serum content a cohesive and ECM-rich fibroblast-sheet. The enhanced ECM deposition at low serum concentration is attributed to the inherently high MMP content in both FBS and HS that resulted in degradation of the deposited collagenous matrix, as a function of serum concentration and time in culture. In accordance to previous observations,[27] high serum content for long culture periods results in ECM degradation, due to the high proteolytic activity of MMPs, a family of enzymes responsible for many developmental processes, including morphogenesis, angiogenesis, collagen metabolism and tissue remodelling.[28] The use of HS not only enables more abundant ECM deposition, due to the lower MMP content, but also avoids issues associated with the use of FBS, such as interspecies transmission of disease and severe immune reactions. This work corroborates previous studies advocating the use of HS for cell-based therapies.[29]

Although the *in vivo* milieu is a highly crowded environment composed of numerous molecules with variable sizes and shapes (a rather polydispersed and heterogeneous setting), protein folding and stability under MMC conditions is solely assessed under homogeneous

conditions and only a few *in vitro* (none has used living human or animal cells; primarily bacteria cytoplasm is used as a model) and *in silico* models have studied polydispersity.[30] As first, using living cells, we provide evidence that macromolecular polydispersity is a key modulator of ECM deposition and identify CR as the most suitable macromolecule for accelerated ECM deposition.

The abundant deposited ECM prohibited detachment of intact living substitutes from commercially available thermal responsive pNIPAAm dishes, whilst a pNIPAAm + pNTBA copolymer allowed for first time the production of dense and cohesive tissue modules with intact cell-cell and cell-ECM junctions; tissue like morphology; and positively upregulated molecular functions, ECM and cellular components and biological processes. In addition to the accelerated and ample ECM deposition, this technology not only requires a lower cell number than multilayer cell sheets, which often not available, but also bypasses the need of multi-layer cell sheets altogether, which due to poor nutrient transport, hypoxia and waste accumulation result in cell necrosis in the central cell-layers.[31]

Further, MMC (75μg/ml CR) facilitated accelerated tissue-specific ECM deposition at low serum concentration (5% FBS) in human tenocyte and osteoblast culture. Possibly, MMC intensifies the efficacy of survival signals, mitogens and growth factors present in sera, making the use of high serum supplementation redundant. This is of significant importance, given that high serum concentration is often associated with phenotypic drift and unintended trans-differentiation.[32]

Here, we provide evidence for the notion that MMC, by imitating native tissue localised density, can be utilised to effectively modulate *in vitro* microenvironments and ultimately produce ECM-rich cell substitutes at low serum concentration, within hours rather than days or months in culture, without compromising fundamental cellular functions.

Experimental Section

Cell culture: Human lung fibroblasts (WI-38; American Tissue Culture Collection), human skin fibroblasts (WS-1; American Tissue Culture Collection) and human tenocytes (DV Biologics) were cultured in Dulbecco's modified Eagle medium (Sigma, Ireland) with 10% foetal bovine serum (FBS) (Sigma, Ireland) and 1% penicillin-streptomycin (Sigma, Ireland) at 37^{o}C in a humidified atmosphere of 5% CO_2. Human osteoblasts (Lonza, UK) were maintained in low-glucose Dulbecco's modified Eagle medium (Sigma, Ireland) and same conditions as above. Cells were seeded at 25,000 cells/cm^2 in 24-well plates and were allowed to attach for 24 hours. After 24 hours the medium was changed with medium containing macromolecular crowders (100μg/ml DxS 500kDa; 37.5mg/ml Ficoll™ 70 and 25mg/ml Ficoll™ 400; and 75μg/ml CR (Sigma, Ireland) with various percentages of FBS (0%, 0.5%, 1%, 2%, 5%, 10% for skin and lung fibroblasts and 0%, 0.5%, 5%, 10% for osteoblasts and tenocytes). To induce collagen synthesis fibroblasts, osteoblasts and tenocytes were supplemented with 100μM L-ascorbic acid phosphate (Sigma, Ireland). After optimisation of culture conditions, commercially available human serum (HS; Lonza, UK) was used as supplement to replace FBS.

Phase contrast microscopy: The influence of various crowders and FBS percentages on cell morphology was evaluated using phase-contrast microscopy at day 2, 4 and 6. Images of the cells were taken using an inverted microscope (Leica microsystem, Germany) and images were analysed with the LAS EZ 2.0.0 software.

Cell metabolic activity (alamarBlue®): alamarBlue® assay (Invitrogen, USA) was performed to quantify the influence of various crowders and serum present on metabolic activity of the fibroblasts, osteoblasts and tenocytes. Briefly, at the end of culture time points, cells were

washed with Hanks' Balanced Salt solution (HBSS, Sigma, Ireland) and then diluted alamarBlue® was added. After 4 hours of incubation at 37ºC, absorbance was measured at 550 and 595nm with help of Varioskan Flash spectral scanning multimode reader (Thermo Scientific). Cell metabolic activity was expressed in terms of reduction percentage of alamarBlue®.

Cell viability (Live/Dead® assay): Live/Dead® assay (Molecular Probes, Invitrogen, USA) was used to measure the influence of various crowders, serum present and thermal responsive polymers on cell viability, as per manufacturer protocol. Briefly, at the end of culture time points, cells were washed with HBSS and then Live/Dead® staining solution was added (2μmol/L calcein-AM-green and 0.5μmol/L ethidium homodimer-1) in a pH-adjusted buffer. The cells were allowed to incubate for 30 minutes at 37°C and 5% CO_2. Fluorescence images were captured with an Olympus IX-81 inverted fluorescence microscope (Olympus Corporation, Tokyo, Japan).

Collagen extraction: At the end of culture time points, culture media were collected into separate vials, whereas cell layers were washed twice with HBSS. Washed cell layer were digested with porcine gastric mucosa pepsin (Sigma, Ireland) in a final concentration of 1mg/ml in 0.5M acetic acid (Sigma, Ireland). Samples were incubated at 37ºC for 2 hours with gentle shaking followed by neutralization with 0.1N sodium hydroxide (Sigma, Ireland).

Sodium dodecyl sulphate-polyacrylamide gel electrophoresis (SDS-PAGE): Cell layer samples were analysed by SDS-PAGE under non-reducing conditions with Mini-Protean 3 (Bio-Rad Laboratories, UK). 100-500μg/ml of bovine collagen type I (Symatese Biomateriaux, France) was used as standards with every gel. Protein bands were stained with the SilverQuest® kit (Invitrogen, USA) according to the manufacturer's protocol. Densitometric analysis of gels was performed using GeneTools analysis software (Syngene,

UK). Collagen bands were quantified by defining each band with the rectangular tool with background subtraction.

Immunocytochemistry: Cells were seeded on 4 or 8-well Lab-Tek™ II (Nunc, Denmark) chamber slides at 25,000 cells/cm^2 and after 24 hours of seeding, cells were treated with crowders. At the end of cell culture time points, medium was removed and cell layers were washed with HBSS and fixed with 2% paraformaldehyde (Sigma, Ireland) at room temperature for 15min. After several washes in phosphate-buffered saline (PBS, Sigma, Ireland), nonspecific sites were blocked with 3% bovine serum albumin (Sigma, Ireland) in PBS for 30 minutes. The cells were incubated for 90min at room temperature or overnight at 4^{o}C simultaneously with the primary antibody of collagen type I, III, IV, V, VI, VII, laminin, elastin, fibronectin, α-smooth muscle actin, tenomodulin, epithelial keratin, tubulin, hyaluronic acid, chondroitin sulphate, keratin sulphate, heparin sulphate, aggrecan, biglycan, decorin, Endosialin / Tumor endothelial marker 1 (TEM-1), lysyl oxidase, transglutaminase-2, fibrillin, and interleukin-10. Bound antibodies were visualised using AlexaFluor®488 chicken anti-rabbit (Invitrogen, USA) and AlexaFluor®555 goat anti-mouse (Invitrogen, USA) 1:400 in PBS for 30 minutes. Post-fixation was done with 2% PFA for 15min. Cell nuclei were counterstained with 4,6-diamidino- 2-phenylindole (DAPI; Invitrogen, USA) and slides were mounted with Vectashield® mounting media (Vector Lab, UK). Images were captured and fluorescence intensity measurements were performed with an Olympus IX-81 inverted fluorescence microscope (Olympus Corporation, Tokyo, Japan).

Gelatin zymography: Zymography was performed to analyse expression of matrix metalloproteinase-2. At the end of cell culture time points, culture media were collected and separated on 10% SDS-PAGE gels containing 1mg/ml gelatin (Sigma-Aldrich, Ireland). After electrophoresis, SDS was removed from the gels by two incubations in 2.5% Triton X-100 for 30 minutes. Gels were incubated overnight at 37°C in 2.5% Triton X-100, 50mM Tris pH 7.4,

5mM $CaCl_2$, 1μM $ZnCl_2$. Gels were then stained for 20min with Coomassie Brilliant Blue (Sigma-Aldrich, Ireland) and destained for 2 hours. Uncultured medium with various percentages of FBS and HS were used as controls.

Dynamic light scattering (DLS) measurements: DLS measurements of macromolecules were carried out using Zetasizer Nano ZS90 (Malvern Instruments, UK) at 25^{o}C. Molecules were dissolved in double distilled water for size measurements (Z-Ave; d.nm) and for zeta (ζ)-potential analysis. The results were analysed using the Zetasizer software 6.12 (Malvern Instruments, UK).

Nanoparticle tracking analysis (NTA): NTA measurements were performed using NanoSight LM10 (NanoSight, Amesbury, UK) equipped with a sample chamber with a 405nm blue laser. The samples were injected in the sample chamber with sterile syringes (BD) until the liquid reached the tip of the nozzle. All measurements were performed at room temperature (26.3°C – 26.5°C). The software used for capturing and analysing the data was the NTA 2.0 Build 127. The samples were measured for 196 - 215s with manual shutter and gain adjustments. The 'single shutter and gain mode' was used to capture the dispersity of the samples based on their viscosity in in mm^2/sec (Centistokes). Three measurements of the same sample were performed for all samples. The mean size and SD values obtained by the NTA software correspond to the arithmetic values calculated with the hydrodynamic sizes of all the particles analysed by the software.

Total protein extraction: Human skin fibroblasts were cultured in 24-well plates (25,000 cells/cm^2). After 24 hours the medium was changed with medium containing macromolecular crowder (75μg/ml CR), 0.5% HS and 100μM L-ascorbic acid phosphate. After 2 days the media were collected and cell layer were washed three times with ice cold PBS. Total protein extraction from cell layer was carried out using Qproteome^{TM} mammalian protein preparation kit (Qiagen, UK). Briefly, cell layers were gently scraped using ice cold PBS and transferred

in to pre-chilled 1.5ml tubes (Protein LoBind Tubes, Eppendorf, UK). The cell suspension was centrifuged for 5 minutes at 450g and 4°C. The supernatant was discarded and pellet was re-suspended in mammalian cell lysis buffer containing Benzonase® nuclease and protease inhibitor, followed by incubation in a rotary shaker for 5 minutes at 4°C. The suspension was centrifuged for 10 minutes at 14,000g and 4°C. The supernatant was transferred into new pre-chilled 1.5 ml tubes (Protein LoBind Tubes, UK).

SDS-PAGE and gel band excision for proteomic analysis: Total protein from cell layer and medium samples were separated on 4-12% Bis-Tris Gels (NuPAGE®Novex®, 1.0-mm thick, 10-well, Invitrogen, UK) under reducing conditions (NuPAGE® reducing agent, Invitrogen, UK) at 70°C for 10min. After reducing the samples, iodoacetamide was added to final concentration of 2mM and incubated for 30 minutes at room temperature in the dark. Gels were run in 1X NuPAGE® MOPS 3-(N-morpholino) propanesulfonic acid SDS running buffer (Invitrogen, UK) containing NuPAGE® antioxidant (Invitrogen, UK) in the upper buffer chambers of XCell SureLock™ Mini-Cell electrophoresis system (Invitrogen, UK). 5μl of precision plus protein standards (Bio-Rad, UK) was used as a molecular weight marker with the range of 250kDa to 10kDa. Protein bands were stained with the Coomassie brilliant blue and destained with destaining solution (40% ethanol, 10% acetic acid and 50% deionized water). Band excision was done in a laminar flow cabinet with the help of light box. Gel bands were excised with scalpel and cut each slice into 1mm cubes and transfer into protein LoBind tubes (Eppendorf, UK). The complete proteomics analysis was carried out at Central Proteomics Facility, Sir William Dunn Pathology School, Oxford University, UK.

Trypsin digestion: Gel lanes were excised and cut into twenty equal portions and digested with trypsin. Briefly the gel bands were distained, reduced with DTT and then alkylated with iodoacetamide. Gel bands were digested with trypsin for 16 hours at 37°C. Peptides were

extracted with sequential washes of acidified aqueous acetonitrile and concentrated in a vacuum centrifuge and then purified.

Mass spectrometry: Samples were run on a LTQ XL Orbitrap mass spectrometer (Thermo Scientific, UK) coupled to an Ultimate 3000 RSLC nano HPLC system (Dionex, UK). The system was run in direct injection using a home-packed 15cm long by 75μm internal diameter picotip emitter (New Objective, UK) containing ReproSil-Pur C18-Aq, 3μm bead (Dr. Maisch GmbH HPLC, Germany). Samples were analysed on a 120min gradient with the mass spectrometer operated in a data dependent acquisition mode in which the top 5 2+, 3+ and 4+ ions was selected for fragmentation.

Proteomics data analysis: All data were analysed in the Central Proteomics Facilities Pipeline (CPFP).[33] Briefly, data were merged from all gel bands in a sample and were searched using Mascot, X!tandem and OMSSA. Results from the search engines were merged and the False Discovery Rate (FDR) calculated. Protein abundance fold changes were estimated using Spectral Index Normalised Quantitation (SINQ) label-free quantitation.

Proteomic validation by immunocytochemistry: To validate proteomics results, proteins of interest were analysed and validated by fluorescence intensity measurements of immunocytochemistry images using protocol described above.

Preparation of cell-matrix sheet using temperature-responsive cell culture surfaces: pNIPAAm and pNTBA were added in anhydrous ethanol in the ratio of 40μg/ml and 20μg/ml and left for continuous shaking overnight. Petri dishes were subsequently coated with the appropriate amount of polymer in a desiccator. The dishes were further dried in vacuum oven at 60^{o}C overnight. Fibroblasts were seeded at 25,000 cells/cm^2 after drying and mild UV sterilization of the petri dishes for 2h. After 24h of seeding, cells were treated with media

containing macromolecular crowder. After 2 days of culture, the fibroblast sheets were harvested by decreasing the temperature of culture to 20^{o}C for 30 minutes.

Scanning electron microscopy (SEM): After 2 days of culture, cell-sheets were washed with HBSS and fixed with 2% paraformaldehyde at room temperature for 15min. Subsequently, the cell-sheets were washed three times with PBS and serially dehydrated with 30%, 50%, 70%, 90% and 100% ethanol. The dehydrated cell-sheets were placed on adhesive carbon tabs mounted on SEM specimen stubs and then were dried. The specimens were subsequently coated with gold using an Emitech K550 coating system. SEM images were obtained using a Hitachi S-4700 field emission microscope operating with a beam voltage of 15KV.

Atomic force microscopy (AFM): WS-1 fibroblasts were seeded on 4-well Lab-Tek™ II chamber slides at 25,000 cells/cm^2 and after 24 hours of seeding, cells were treated with crowders. After 2 days of culture, medium was removed and cell layers were washed with HBSS and fixed with 2% paraformaldehyde at room temperature for 15 min. The cell layers were washed three times with phosphate-buffered saline (PBS) and serially dehydrated with 30%, 50%, 70%, 90% and 100% ethanol. AFM was performed on a commercial microscope (MFP-3D, Asylum Research) using triangular cantilevers (DNP C, Bruker) each having a nominal resonance frequency of 56 KHz and a spring constant of 0.24 N/m. Images were recorded using contact mode in an ambient environment after drying the sample with nitrogen gas. Images recorded using amplitude modulation mode yielded similar results, as did images recorded in PBS on samples, which remained fully hydrated. All images were first-order XY plane-fit flattened (Igor Pro, Wavemetrics) except for **Supplementary Fig. 17f, 18c**, which were also zero-order line-by-line flattened along the fast scan direction (X).

Masson's Trichrome staining: Cell-sheets were fixed in Bouin's solution for 1 hour at 56^{o}C. After rinsing running tap water it was stained in Weigert's iron haematoxylin working solution for 10 minutes and then stained in biebrich scarlet-acid fuchsin solution. Cell-sheets

were differentiated in phosphomolybdic-phosphotungstic acid solution and then directly (without rinse) transferred to aniline blue solution. After brief rinse in distilled water, it was differentiated in 1% acetic acid solution. Washing in distilled water followed by dehydration through a series of ethanol baths (70%, 80%, 90%, 100%). The final dehydration step was carried out in xylene for least 5 minutes and the slides were mounted using DPX. Images were captured with an Olympus IX-81 inverted microscope.

Picro-Sirius red staining: Cell-sheets were stained with Weigert's haematoxylin for 8 minutes and then rinsing in tap water it was stained with 0.2% phosphomolybdic acid hydrate. After rinsing in distilled water, the cell-sheets were stained with Picro-Sirius Red followed by wash in acidified water. Dehydration was done through a series of ethanol baths (70%, 80%, 90%, 100%). The final dehydration step was carried out in xylene for least 5 minutes and the slides were mounted using DPX. Images were captured with an Olympus IX-81 inverted microscope.

Statistical analyses: Numerical data is expressed as mean ± SD. Analysis was performed using statistical software (MINITAB^{TM} version 16, Minitab Inc., USA). One way analysis of variance (ANOVA) for multiple comparisons and 2-sample t-test for pair wise comparisons were employed after confirming the following assumptions: (a) the distribution from which each of the samples was derived was normal (Anderson-Darling normality test); and (b) the variances of the population of the samples were equal to one another (Bartlett's and Levene's tests for homogenicity of variance). Non-parametric statistics were used when either or both of the above assumptions were violated and consequently Kruskal-Wallis test for multiple comparisons or Mann-Whitney test for 2-samples were carried out. Statistical significance was accepted at $p<0.05$. Experiments were performed in triplicate or quadruplicate.

Supporting Information: Supporting Information is available online from the Wiley Online Library or from the author.

Acknowledgements: We thank Dr Oliver Carroll for laboratory management; and Mr Maciek Doczyk (http://doczykdesign.com) for his support in the preparation of Figure 1 of this manuscript. This work is supported by Science Foundation Ireland, Research Frontiers Programme, Project Number: SFI-09-RFP-ENM2483 to D.Z.; Science Foundation Ireland, E.T.S. Walton Visitor Awards Programme, Project Number: 08/W.1/B2568 to M.R., A.P. and D.Z.; Health Research Board, Project Number: HRA_POR/2011/84 to D.Z.; and College of Engineering and Informatics, Postgraduate Scholarship Scheme, NUI Galway to P.K. and D.Z.

Received: ((will be filled in by the editorial staff))

Revised: ((will be filled in by the editorial staff))

Published online: ((will be filled in by the editorial staff))

[1] (a) A. Dove, Nature Biotechnology 2002, 20, 339; (b) O. Lindvall, Z. Kokaia, A. Martinez-Serrano, Nature Medicine 2004, 10, S42; (c) E. D. Adler, T. M. Maddox, Nature Reviews Cardiology 2007, 4, 2; (d) A. P. Chidgey, D. Layton, A. Trounson, R. L. Boyd, Nature 2008, 453, 330.

[2] (a) E. D. Thomas, New England Journal of Medicine 1978, 298, 963; (b) B. Speck, M. M. Bortin, R. Champlin, J. M. Goldman, R. H. Herzig, P. B. McGlave, H. A. Messner, R. S. Weiner, A. A. Rimm, The Lancet 1984, 1, 665; (c) E. Tateishi-Yuyama, H. Matsubara, T. Murohara, U. Ikeda, S. Shintani, H. Masaki, K. Amano, Y. Kishimoto, K. Yoshimoto, H. Akashi, K. Shimada, T. Iwasaka, T. Imaizumi, The Lancet 2002, 360, 427.

[3] (a) N. Matsuda, T. Shimizu, M. Yamato, T. Okano, Advanced Materials 2007, 19, 3089; (b) J. van Ramshorst, S. Rodrigo, M. Schalij, S. Beeres, J. Bax, D. Atsma, Journal of Cardiovascular Translational Research 2011, 4, 182.

[4] (a) E. Bell, B. Ivarsson, C. Merrill, Proceedings of the National Academy of Sciences 1979, 76, 1274; (b) E. Bell, H. Ehrlich, D. Buttle, T. Nakatsuji, Science 1981, 211, 1052; (c) E. Bell, S. Sher, B. Hull, C. Merrill, S. Rosen, A. Chamson, D. Asselineau, L. Dubertret, B. Coulomb, C. Lapiere, B. Nusgens, Y. Neveux, Journal of Investigative Dermatology 1983, 81, 2s; (d) G. G. Gallico, N. E. O'Connor, C. C. Compton, O. Kehinde, H. Green, New England Journal of Medicine 1984, 311, 448; (e) J. Nanchahal, R. Dover, W. Otto, S. Dhital, The Lancet 1989, 334, 191.

[5] C. Weinberg, E. Bell, Science 1986, 231, 397.

[6] (a) L. Tang, J. Eaton, American Journal of Clinical Pathology 1995, 103, 466; (b) B. Nilsson, K. N. Ekdahl, T. E. Mollnes, J. D. Lambris, Molecular Immunology 2007, 44, 82; (c) J. M. Anderson, A. Rodriguez, D. T. Chang, Seminars in Immunology 2008, 20, 86; (d) C. A. N. Broekhuizen, L. de Boer, K. Schipper, C. D. Jones, S. Quadir, R. G. Feldman, C. M. J. E. Vandenbroucke-Grauls, S. A. J. Zaat, Biomaterials 2009, 30, 6444; (e) G. Wick, A. Backovic, E. Rabensteiner, N. Plank, C. Schwentner, R. Sgonc, Trends in Immunology 2010, 31, 110.

[7] (a) J. Yang, M. Yamato, K. Nishida, T. Ohki, M. Kanzaki, H. Sekine, T. Shimizu, T. Okano, Journal of Controlled Release 2006, 116, 193; (b) J. Yang, M. Yamato, T. Shimizu, H. Sekine, K. Ohashi, M. Kanzaki, T. Ohki, K. Nishida, T. Okano, Biomaterials 2007, 28, 5033.

[8] M. Peck, N. Dusserre, T. N. McAllister, N. L'Heureux, Mater Today 2011, 14, 218.

[9] (a) J. G. Rheinwatd, H. Green, Cell 1975, 6, 331; (b) H. Green, O. Kehinde, J. Thomas, Proceedings of the National Academy of Sciences 1979, 76, 5665; (c) N. E. O'Connor, J. B. Mulliken, S. Banks-Schlegel, O. Kehinde, H. Green, The Lancet 1981, 317, 75.

[10] (a) N. L'Heureux, L. Germain, R. Labbe, F. A. Auger, Journal of Vascular Surgery 1993, 17, 499; (b) N. L'Heureux, S. Paquet, R. Labbe, L. Germain, F. A. Auger, The Journal

of the Federation of American Societies for Experimental Biology 1998, 12, 47; (c) N. L'Heureux, T. N. McAllister, L. M. de la Fuente, New England Journal of Medicine 2007, 357, 1451; (d) G. Konig, T. N. McAllister, N. Dusserre, S. A. Garrido, C. Iyican, A. Marini, A. Fiorillo, H. Avila, W. Wystrychowski, K. Zagalski, M. Maruszewski, A. L. Jones, L. Cierpka, L. M. de la Fuente, N. L'Heureux, Biomaterials 2009, 30, 1542.

[11] N. L'Heureux, N. Dusserre, G. Konig, B. Victor, P. Keire, T. N. Wight, N. A. F. Chronos, A. E. Kyles, C. R. Gregory, G. Hoyt, R. C. Robbins, T. N. McAllister, Nature Medicine 2006, 12, 361.

[12] M. Griffith, R. Osborne, R. Munger, X. Xiong, C. J. Doillon, N. L. C. Laycock, M. Hakim, Y. Song, M. A. Watsky, Science 1999, 286, 2169.

[13] K. Nishida, M. Yamato, Y. Hayashida, K. Watanabe, K. Yamamoto, E. Adachi, S. Nagai, A. Kikuchi, N. Maeda, H. Watanabe, T. Okano, Y. Tano, New England Journal of Medicine 2004, 351, 1187.

[14] (a) T. Shimizu, M. Yamato, A. Kikuchi, T. Okano, Biomaterials 2003, 24, 2309; (b) Y. Miyahara, N. Nagaya, M. Kataoka, B. Yanagawa, K. Tanaka, H. Hao, K. Ishino, H. Ishida, T. Shimizu, K. Kangawa, S. Sano, T. Okano, S. Kitamura, H. Mori, Nature Medicine 2006, 12, 459; (c) S. Masuda, T. Shimizu, M. Yamato, T. Okano, Advanced Drug Delivery Reviews 2008, 60, 277.

[15] M. A. Nandkumar, M. Yamato, A. Kushida, C. Konno, M. Hirose, A. Kikuchi, T. Okano, Biomaterials 2002, 23, 1121.

[16] K. Ohashi, T. Yokoyama, M. Yamato, H. Kuge, H. Kanehiro, M. Tsutsumi, T. Amanuma, H. Iwata, J. Yang, T. Okano, Y. Nakajima, Nature Medicine 2007, 13, 880.

[17] R. P. Pirraco, H. Obokata, T. Iwata, A. P. Marques, S. Tsuneda, M. Yamato, R. L. Reis, T. Okano, Tissue Engineering Part A 2011, 17, 1507.

[18] (a) N. E. Vrana, N. Builles, V. Justin, J. Bednarz, G. Pellegrini, B. Ferrari, O. Damour, D. J. S. Hulmes, V. Hasirci, Investigative Ophthalmology & Visual Science 2008, 49, 5325;

(b) R. Ren, A. E. K. Hutcheon, X. Q. Guo, N. Saeidi, S. A. Melotti, J. W. Ruberti, J. D. Zieske, V. Trinkaus-Randall, Developmental Dynamics 2008, 237, 2705.

[19] T. Ide, K. Nishida, M. Yamato, T. Sumide, M. Utsumi, T. Nozaki, A. Kikuchi, T. Okano, Y. Tano, Biomaterials 2006, 27, 607.

[20] J. Campisi, F. Fagagna, Nature Reviews Molecular Cell Biology 2007, 8, 729; A. Beltrami, D. Cesselli, C. Beltrami, Clinical Pharmacology & Therapeutics 2012, 91, 21.

[21] (a) S. B. Zimmerman, B. Harrison, Proceedings of the National Academy of Sciences 1987, 84, 1871; (b) A. P. Minton, G. C. Colclasure, J. C. Parker, Proceedings of the National Academy of Sciences 1992, 89, 10504; (c) S. B. Zimmerman, A. P. Minton, Annu Rev Bioph Biom 1993, 22, 27; (d) B. van den Berg, R. J. Ellis, C. M. Dobson, The European Molecular Biology Organization Journal 1999, 18, 6927; (e) L. A. Munishkina, E. M. Cooper, V. N. Uversky, A. L. Fink, Journal of Molecular Recognition 2004, 17, 456; (f) R. R. Lareu, K. H. Subramhanya, Y. Peng, P. Benny, C. Chen, Z. Wang, R. Rajagopalan, M. Raghunath, Federation of European Biochemical Societies Letters 2007, 581, 2709; (g) R. R. Lareu, K. S. Harve, M. Raghunath, Biochemical and Biophysical Research Communications 2007, 363, 171; (h) R. R. Lareu, I. Arsianti, H. K. Subramhanya, P. Yanxian, M. Raghunath, Tissue Engineering 2007, 13, 385; (i) L. A. Munishkina, A. Ahmad, A. L. Fink, V. N. Uversky, Biochemistry 2008, 47, 8993; (j) K. Harve, R. Vigneshwar, R. Rajagopalan, M. Raghunath, Proceedings of the National Academy of Sciences 2008, 105, 119; (k) Z. Zhou, J.-B. Fan, H.-L. Zhu, F. Shewmaker, X. Yan, X. Chen, J. Chen, G.-F. Xiao, L. Guo, Y. Liang, Journal of Biological Chemistry 2009, 284, 30148; (l) C. Chen, F. Loe, A. Blocki, Y. Peng, M. Raghunath, Advanced Drug Delivery Reviews 2011, 63, 277; (m) D. I. Zeugolis, A. Satyam, *EP. 2532736,* 2012.

[22] E. G. Canty, K. E. Kadler, Journal of Cell Science 2005, 118, 1341.

[23] (a) N. Matsuda, T. Shimizu, M. Yamato, T. Okano, Advanced Materials 2007, 19, 3089; (b) Y. Haraguchi, T. Shimizu, T. Sasagawa, H. Sekine, K. Sakaguchi, T. Kikuchi, W.

Sekine, S. Sekiya, M. Yamato, M. Umezu, T. Okano, Nature Protocols 2012, 7, 850; (c) K. A. Athanasiou, R. Eswaramoorthy, P. Hadidi, J. C. Hu, Annual Review of Biomedical Engineering 2013, 15, 115.

[24] (a) K. R. Stevens, K. L. Kreutziger, S. K. Dupras, F. S. Korte, M. Regnier, V. Muskheli, M. B. Nourse, K. Bendixen, H. Reinecke, C. E. Murry, Proceedings of the National Academy of Sciences 2009, 106, 16568; (b) H. Sekine, T. Shimizu, I. Dobashi, K. Matsuura, N. Hagiwara, M. Takahashi, E. Kobayashi, M. Yamato, T. Okano, Tissue Engineering Part A 2011, 17, 2973; (c) G. Forte, S. Pietronave, G. Nardone, A. Zamperone, E. Magnani, S. Pagliari, F. Pagliari, C. Giacinti, C. Nicoletti, A. Musaró, M. Rinaldi, M. Ribezzo, C. Comoglio, E. Traversa, T. Okano, M. Minieri, M. Prat, P. Di Nardo, Stem Cells 2011, 29, 2051.

[25] D. Cigognini, A. Lomas, P. Kumar, A. Satyam, A. English, A. Azeem, A. Pandit, D. Zeugolis, Drug Discovery Today In Press.

[26] R. J. Ellis, A. P. Minton, Nature 2003, 425, 27.

[27] B. H. Strauss, R. Robinson, W. B. Batchelor, R. J. Chisholm, G. Ravi, M. K. Natarajan, R. A. Logan, S. R. Mehta, D. E. Levy, A. M. Ezrin, F. W. Keeley, Circulation Research 1996, 79, 541.

[28] T. H. Vu, Z. Werb, Genes & Development 2000, 14, 2123.

[29] (a) B. Lindroos, K. Aho, H. Kuokkanen, S. Räty, H. Huhtala, R. Lemponen, O. Yli-Harja, R. Suuronen, S. Miettinen, Tissue Engineering Part A 2010, 16, 2281; (b) A. Aldahmash, M. Haack-Sørensen, M. Al-Nbaheen, L. Harkness, B. Abdallah, M. Kassem, Stem Cell Reviews and Reports 2011, 7, 860.

[30] (a) B. Zhou, Y. Liang, F. Du, Z. Zhou, J. Chen, J Biol Chem 2004, 279, 55109; (b) F. Du, Z. Zhou, Z. Mo, J. Shi, J. Chen, Y. Liang, J Mol Biol 2006, 364, 469; (c) H. X. Zhou, Proteins 2008, 72, 1109; (d) A. Christiansen, Q. Wang, A. Samiotakis, M. S. Cheung, P. Wittung-Stafshede, Biochemistry 2010, 49, 6519; (e) J. Mittal, R. B. Best, Biophysical

journal 2010, 98, 315; (f) B. R. Jefferys, L. A. Kelley, M. J. E. Sternberg, Journal of Molecular Biology 2010, 397, 1329; (g) Q. Wang, M. S. Cheung, Biophysical Journal 2012, 102, 2353; (h) E. J. Cho, J. S. Kim, Biophysical Journal 2012, 103, 424; (i) A. Kudlay, M. S. Cheung, D. Thirumalai, The Journal of Physical Chemistry B 2012, 116, 8513.

[31] T. Shimizu, H. Sekine, J. Yang, Y. Isoi, M. Yamato, A. Kikuchi, E. Kobayashi, T. Okano, The Journal of the Federation of American Societies for Experimental Biology 2006, 20, 708.

[32] (a) G. A. Preston, J. E. Lang, R. R. Maronpot, J. C. Barrett, Cancer Research 1994, 54, 4214; (b) T. Kawakita, E. M. Espana, H. He, R. Smiddy, J.-M. Parel, C.-Y. Liu, S. C. G. Tseng, Investigative Ophthalmology & Visual Science 2006, 47, 1918; (c) A. Parker, H. Shang, M. Khurgel, A. Katz, Cytotherapy 2007, 9, 637; (d) J. Girdlestone, V. Limbani, A. Cutler, C. Navarrete, Cytotherapy 2009, 11, 738; (e) K. Imada, M. Taniguchi, T. Sato, T.-i. Kosaka, K. Yamamoto, A. Ito, J Tokyo Med Univ 2013, 71, 143; (f) Y. Hu, J. Ji, J. Xia, P. Zhao, X. Fan, Z. Wang, X. Zhou, M. Luo, P. Gu, Neurosci Lett 2013, 534, 90; (g) G. Gstraunthaler, T. Lindl, J. Valk, Cytotechnology In Press.

[33] D. C. Trudgian, B. Thomas, S. J. McGowan, B. M. Kessler, M. Salek, O. Acuto, Bioinformatics 2010, 26, 1131.

Figure 1. Modulation of the *in vitro* microenvironment using MMC to imitate the *in vivo* dense extracellular space. **(a)** The deposition of ECM in the current, notably dilute and far from physiological, culturing systems is very slow. In the case of collagen type I, the most abundant ECM protein, cells will produce procollagen and the specific *N*- and *C*- proteinases. However, in the very dilute *in vitro* microenvironment, the conversion of the water-soluble procollagen to insoluble collagen will be very slow since either the proteinases will be deactivated before they cleave the specific *N*- and *C*- propeptides or the procollagen will be dissolved before its conversion to collagen. Only after prolonged culture time, the cells will self-crowd the media and collagen deposition will be achieved. **(b)** Here, we hypothesise that the addition of inert polydispersed macromolecules, presented as spheres with different diameters, in the culture media will create most effective volume occupancy, and will consequently increase the relative density of procollagen and proteinases in the culture media. This will facilitate the cleavage of the propeptides by their respectful proteinases and will lead to the fast procollagen conversion to collagen and deposition of the former.

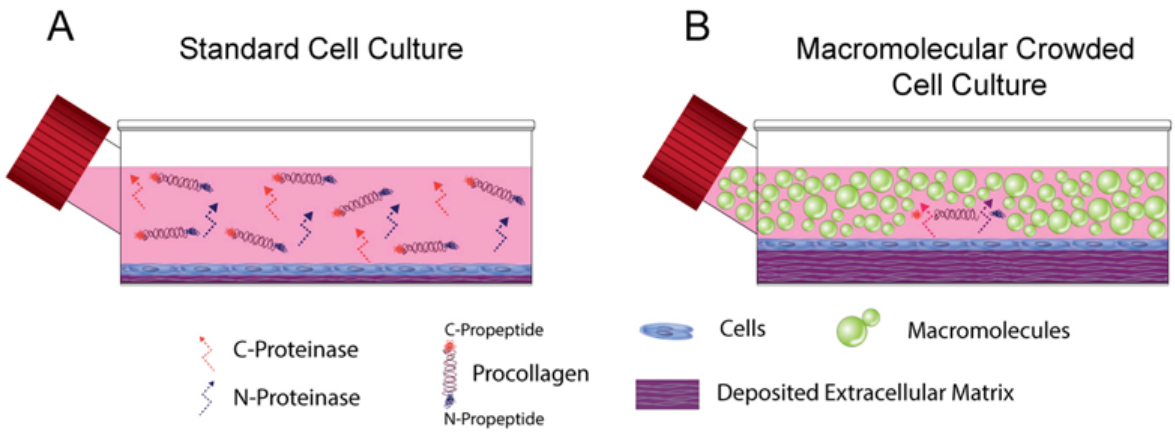

Figure 2. WI38 lung fibroblasts in the presence of DxS and low FBS concentration induced the highest collagen type I deposition after only 2 days in culture. **(a)** Densitometric analysis demonstrated that WI38 fibroblasts in the presence of 100μg/ml 500kDa DxS deposited the highest (p<0.0001) amount of collagen I after 2 days in culture in the presence of 0.5% FBS. Standard (STD): 100μg/ml collagen type I. **(b)** As the FBS concentration was increased, the collagen type I content was found to decrease. Gelatin zymography detected multiple forms of gelatinolytic enzymes; the 68-72kDa identified as proMMP-2, whilst the 62kDa identified as the active form. Both forms of enzyme were found to increase as the FBS concentration was increased. **(c)** ICC experimentation after 2 days in culture confirmed the high deposition of collagen type I, in the presence of DxS, and the reduction in collagen content as a function of increased FBS concentration. It also confirmed high deposition of collagen type I at low FBS concentrations, however fibronectin deposition was not altered, as a function of FBS concentration.

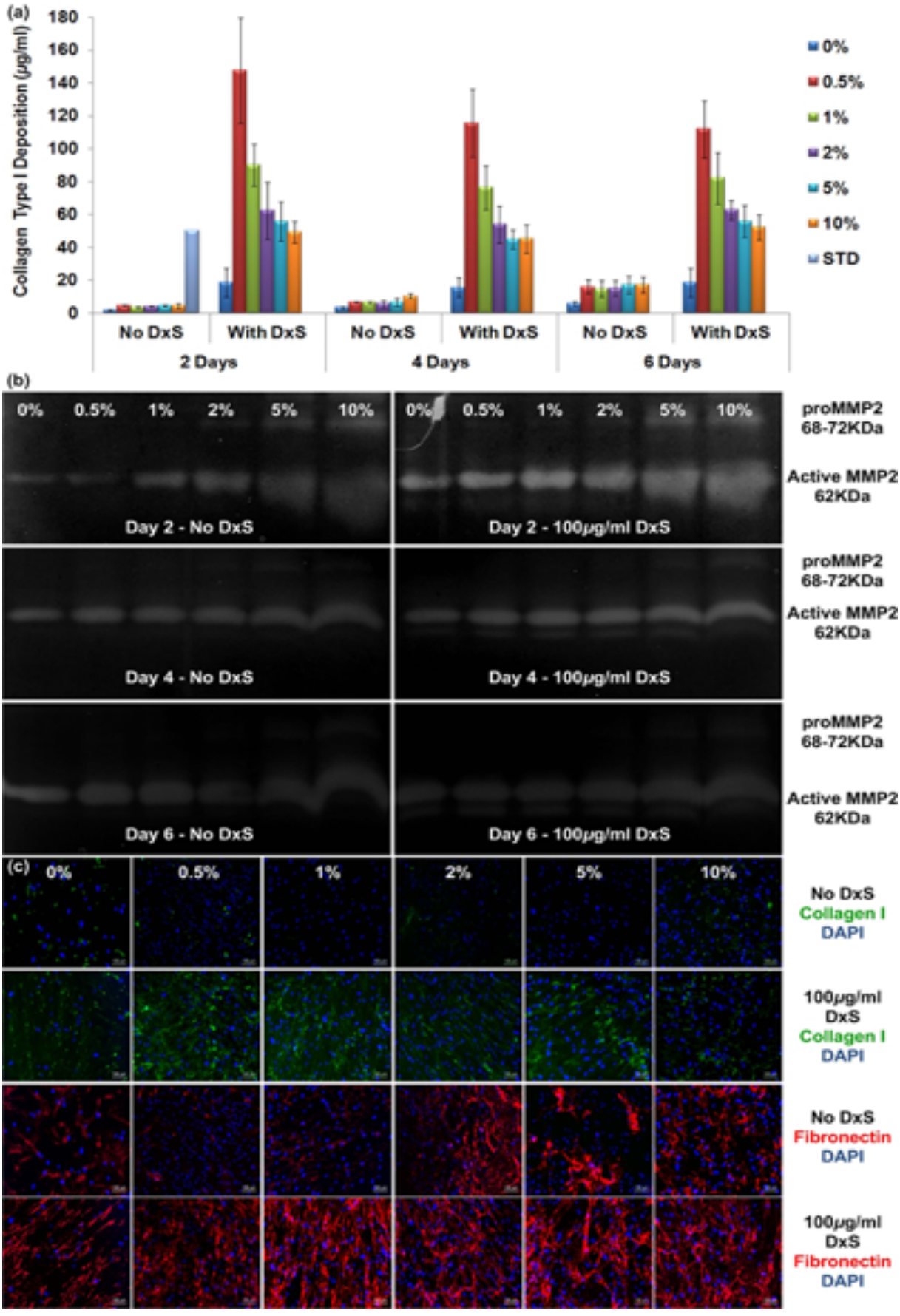
(a)
Collagen Type I Deposition (µg/ml)
180
160
140
120
100
80
60
40
20
0
No DxS
With DxS
No DxS
With DxS
No DxS
With DxS
2 Days
4 Days
6 Days
0%
0.5%
1%
2%
5%
10%
STD
(b)
0%
0.5%
1%
2%
5%
10%
Day 2 - No DxS
Day 2 - 100µg/ml DxS
Day 4 - No DxS
Day 4 - 100µg/ml DxS
Day 6 - No DxS
Day 6 - 100µg/ml DxS
proMMP2
68-72KDa
Active MMP2
62KDa
(c)
No DxS
Collagen I
DAPI
100µg/ml
DxS
Collagen I
DAPI
No DxS
Fibronectin
DAPI
100µg/ml
DxS
Fibronectin
DAPI

Figure 3. Macromolecular polydispersity modulates ECM deposition. **(a)** High-resolution particle size distribution and Nanoparticle Tracking Analysis (NTA) demonstrated that 75μg/ml of CR had significant higher size dispersion (ranges from 10nm to 2μm) than any other macromolecule tested. **(b)** Complementary densitometric analysis of SDS-PAGE (**Supplementary Fig. S11**) demonstrated that WI-38 and WS-1 fibroblasts in the presence of 75μg/ml carrageenan deposited the highest (p<0.0001) amount of collagen I after 2 days in culture supplemented with 0.5% FBS or HS. **(c)** ICC experimentation after 2 days in culture confirmed the high deposition of collagen type I in the presence of MMC.

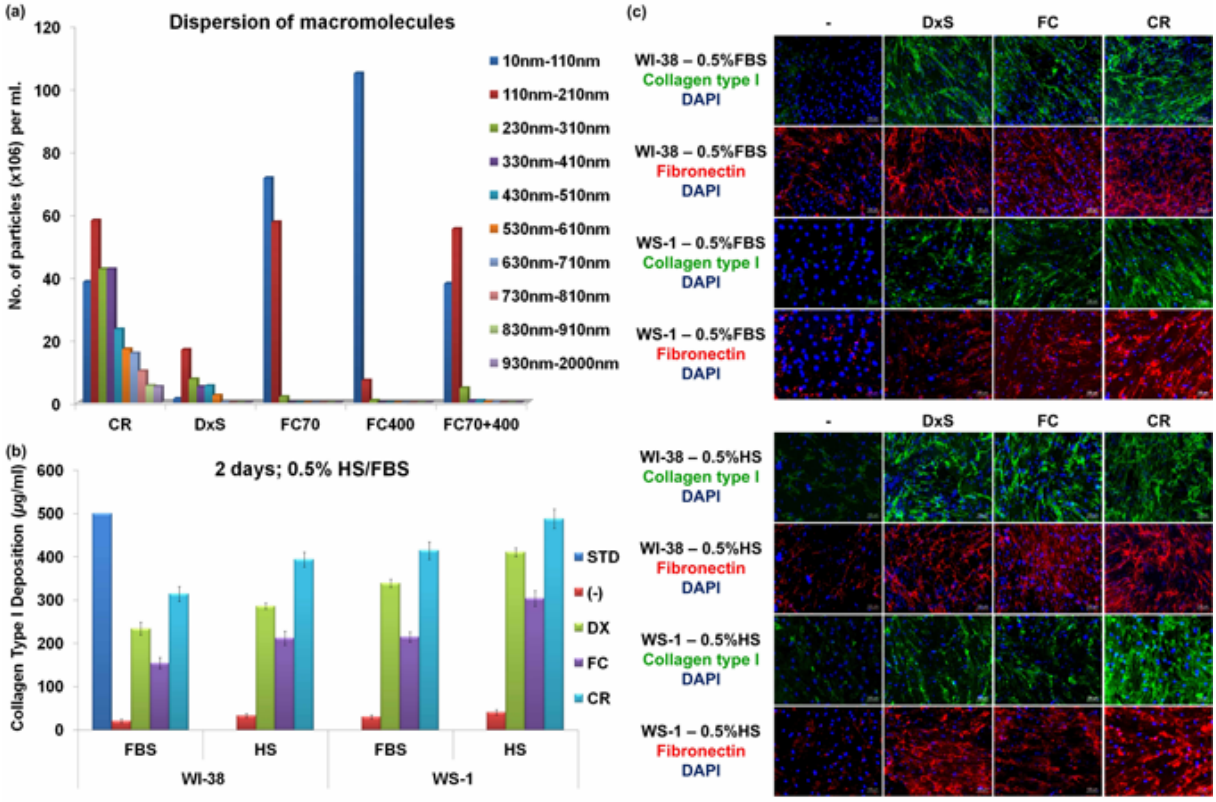

Figure 4. ECM-rich fibroblast-sheet detachment and characterisation after MMC treatment with 75μg/ml CR, 2 days in culture and 0.5% HS. **(a)** pNIPAAm alone was not able to detach the rich in ECM cell sheet. A pNIPAAm + PNTBA copolymer allowed attachment **(b)** and detachment of intact rich in ECM cell sheets **(c)**. ICC analysis clearly demonstrates a less cohesive ECM patent in the absence of CR **(d-f)**, whilst the abundant and fibrillar in nature deposited ECM is evidenced in the presence of CR **(i-k)**. Picro Sirius red **(l, o)** staining further corroborates the high amount of deposited ECM in the presence of CR. SEM analysis **(m, p)** revealed a dense ECM patent of the cell sheets produced under MMC conditions. Representative AFM images **(n, q)** of intercellular regions on the surface of the cell sheet illustrated the presence of a fibrous network under MMC conditions (Z scale, 100 nm for **(n)** and **(q)**).

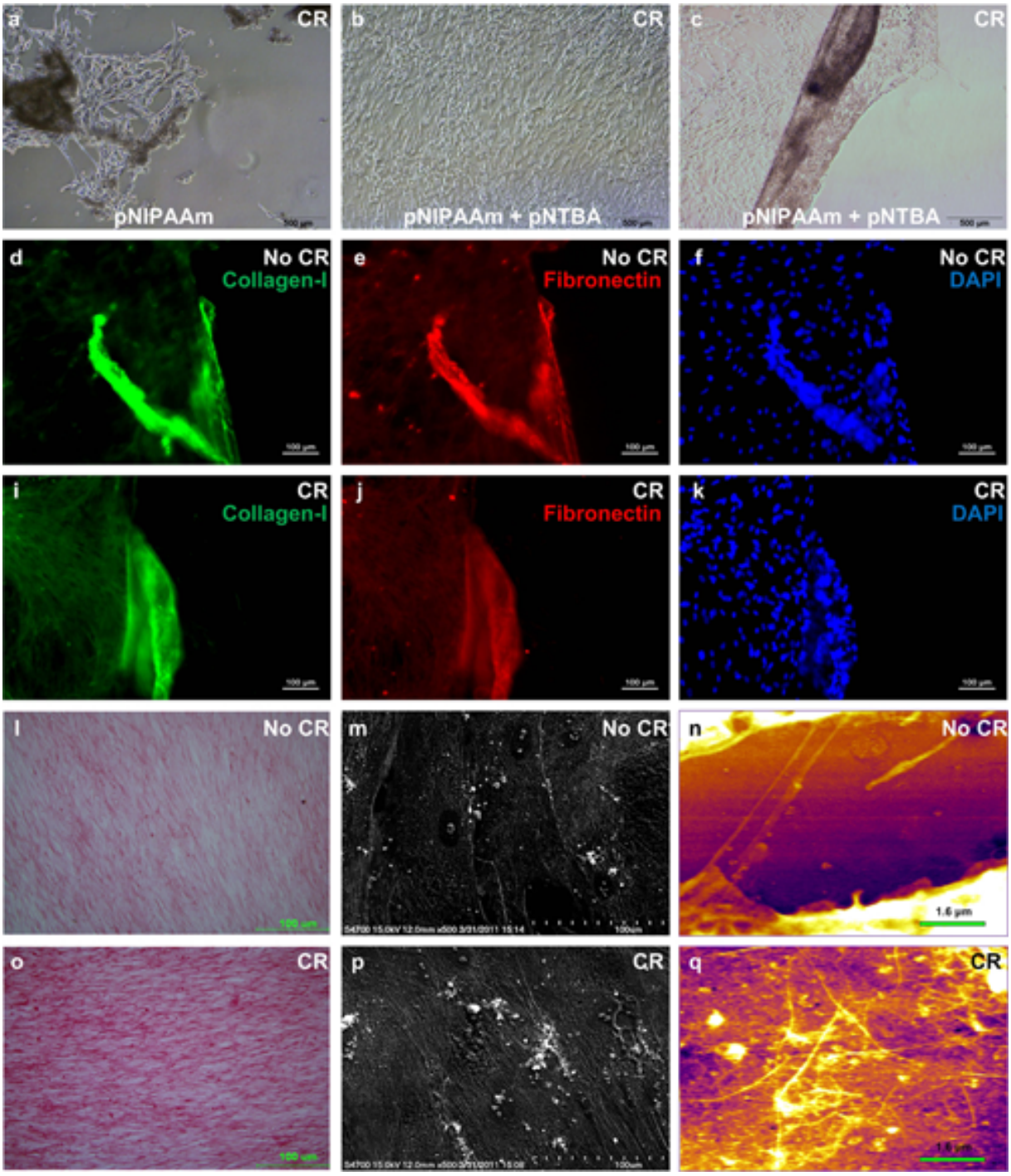
a
CR
pNIPAAm
b
CR
pNIPAAm + pNTBA
c
CR
pNIPAAm + pNTBA
d
No CR
Collagen-I
e
No CR
Fibronectin
f
No CR
DAPI
i
CR
Collagen-I
j
CR
Fibronectin
k
CR
DAPI
l
No CR
m
No CR
n
No CR
1.6 µm
o
CR
p
CR
q
CR

Figure 5. MMC enhances deposition of numerous ECM molecules. **(a)** Immunocytochemistry analysis and **(b)** complementary fluorescence intensity measurements confirmed significantly higher level (p<0.0001) of collagenous proteins (type I, III, IV, V, and VI), basement membrane proteins (e.g. laminin), glycoproteins (e.g. fibronectin), glycosaminoglycans (hyaluronic acid), proteoglycans (decorin), and enzymes (lysyl oxidase) under MMC conditions.

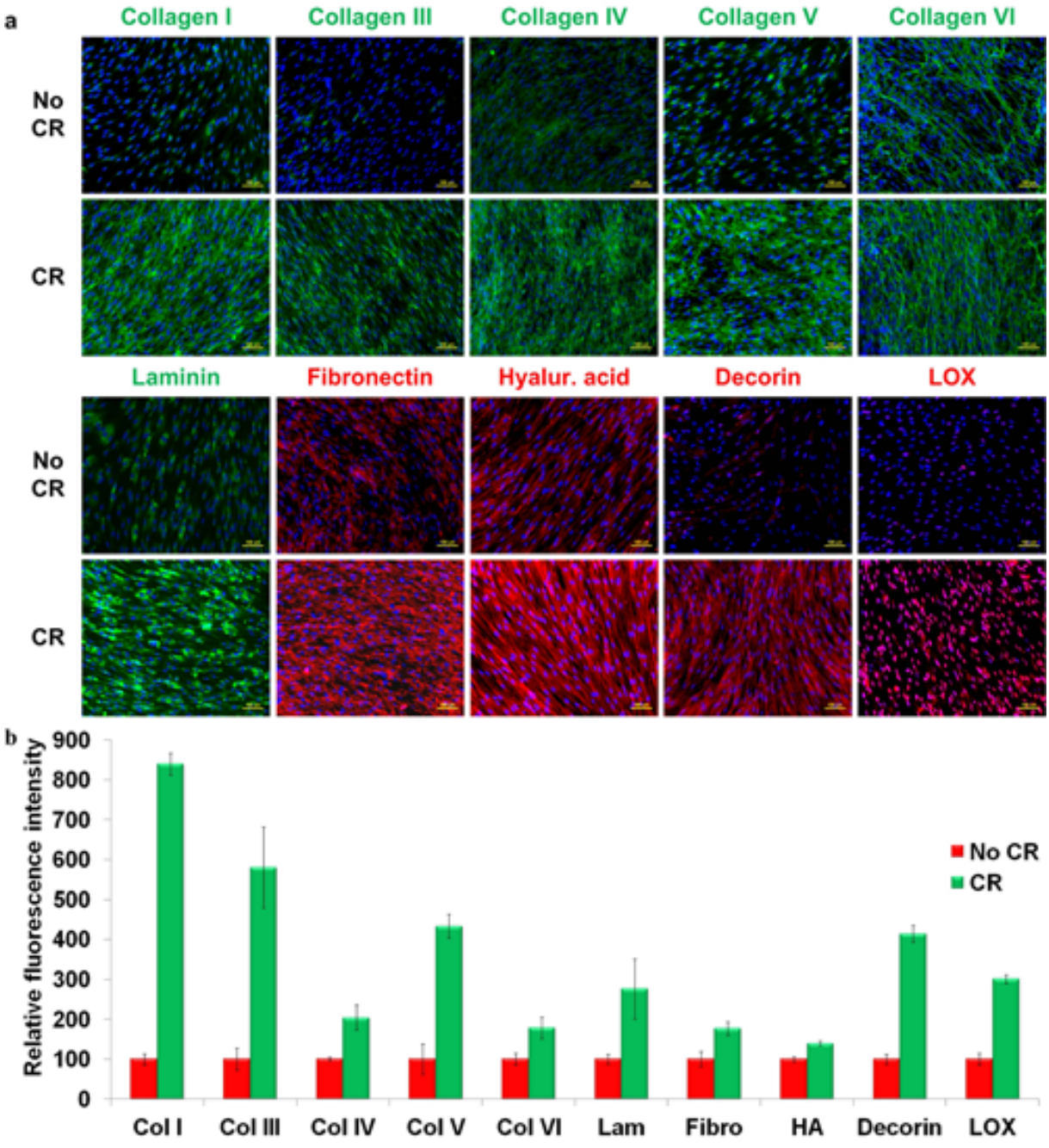

Figure 6. MMC can be readily applied to other cell types to induce high ECM deposition. **(a)** Densitometric analysis of SDS-PAGE (**Supplementary Fig. S19**) demonstrated that human tenocytes in the presence of 75μg/ml CR deposited the highest (p<0.0001) amount of collagen I after 6 days at 5% FBS. Standard (STD): 100μg/ml collagen type I. **(b)** ICC experimentation confirmed the high deposition of collagenous proteins (collagen type I, III, IV, V and VI), glycoproteins (e.g. fibronectin) and basement membrane proteins (e.g. laminin), whilst tenomodulin expression remained unaffected. **(c)** Densitometric analysis of SDS-PAGE (**Supplementary Fig. S20**) demonstrated that human osteoblasts in the presence of 75μg/ml CR deposited the highest (p<0.0001) amount of collagen I after 4 days at 5% FBS. Standard (STD): 100μg/ml collagen type I. **(d)** ICC experimentation confirmed the high deposition of collagenous proteins (collagen type I, III, IV, V and VI), glycoproteins (e.g. fibronectin) and basement membrane proteins (e.g. laminin), whilst tenomodulin expression remained unaffected.

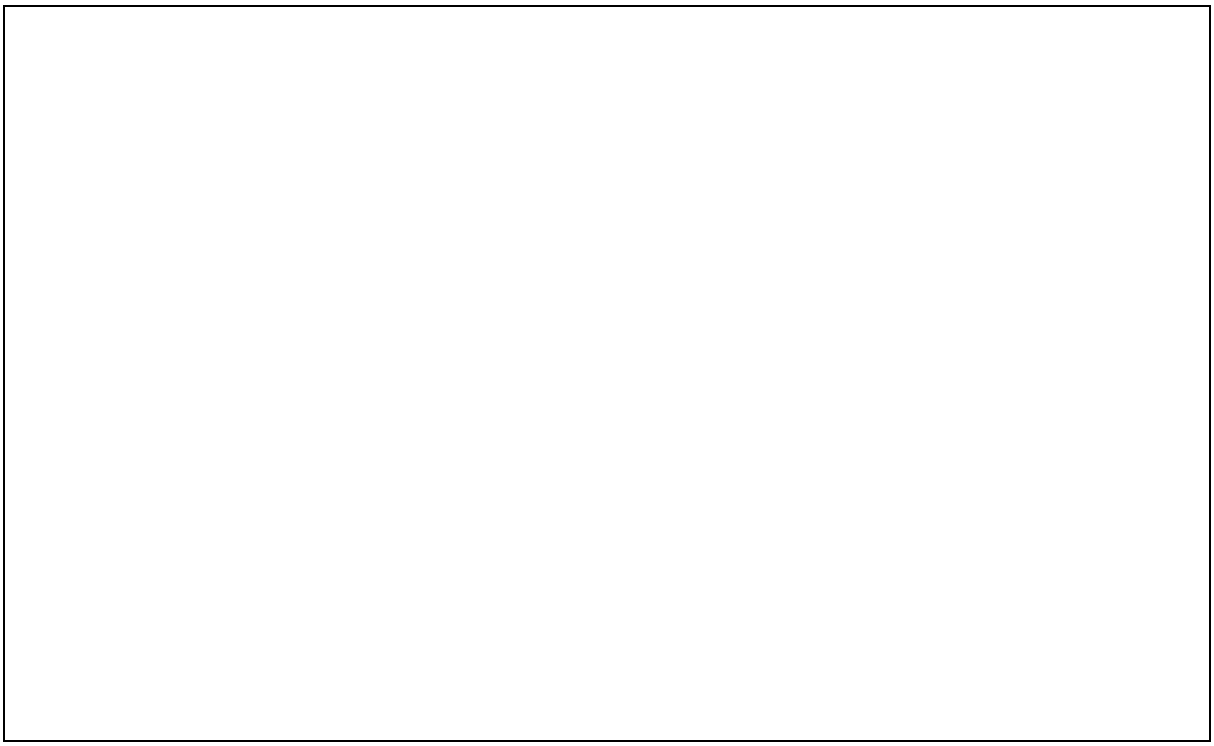

Table of contents entry:

MMC, the addition of inert polydispersed macromolecules in the culture media, effectively emulates the dense *in vivo* extracellular space, resulting in amplified deposition of ECM *in vitro* and subsequent production of cohesive, ECM-rich living substitutes.

Keywords:

Macromolecular crowding, macromolecular polydispersity, excluding volume effect, extracellular matrix deposition, cell-sheet tissue engineering

Authors:

A. Satyam, P. Kumar, X. Fan, A. Gorelov, Y. Rochev, L. Joshi, H. Peinado, D. Lyden, B. Thomas, B. Rodriguez, M. Raghunath, A. Pandit and D. Zeugolis[*]

Title:

Macromolecular crowding meets tissue engineering by self-assembly: A paradigm shift in regenerative medicine

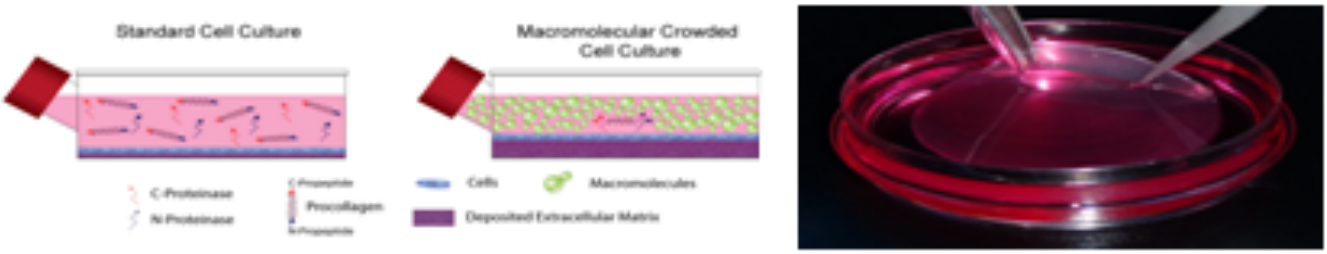

Supplementary Fig S1 SDS-PAGE and complementary densitometric analysis (**Fig. 2a**) revealed that the maximum collagen type I deposition was achieved after culturing WI38 human lung fibroblasts for 2 days at 0.5% foetal bovine serum (FBS) in the presence of 100μg/ml 500kDa Dextran Sulphate (DxS).

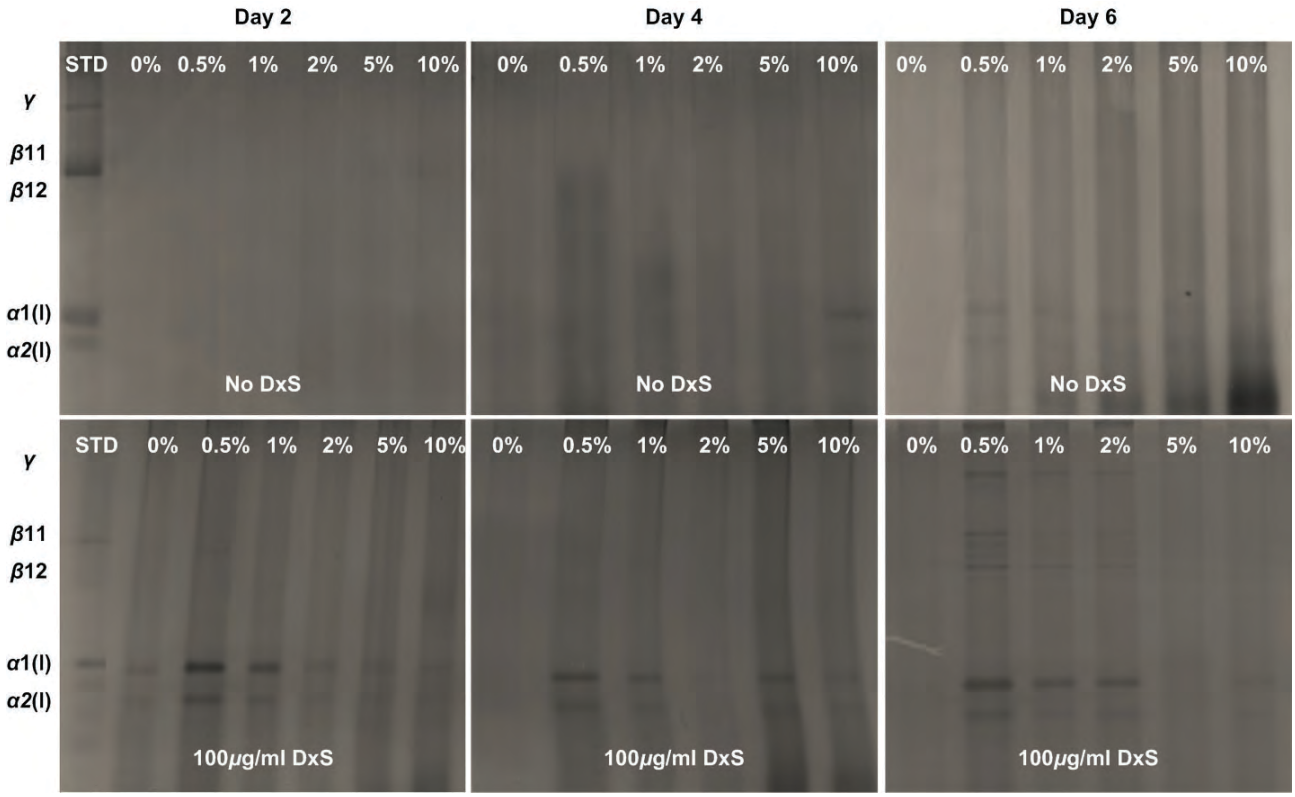

Supplementary Fig S2 Zymography analysis of FBS and HS demonstrate the inherently high MMP content of sera.

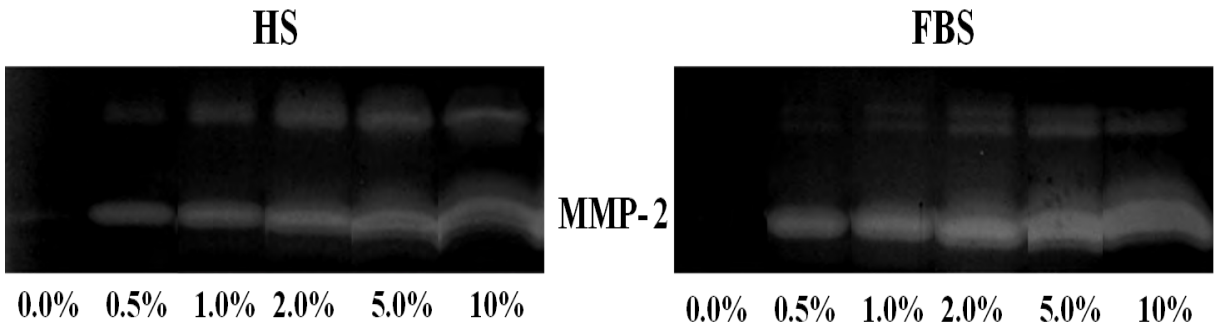

Supplementary Fig S3 SDS-PAGE and complementary densitometric analysis showed that WS1 human skin fibroblasts also deposit the highest amount (p<0.0001) of collagen type I in the presence of 100μg/ml 500kDa DxS at 0.5% FBS after 2 days in culture.

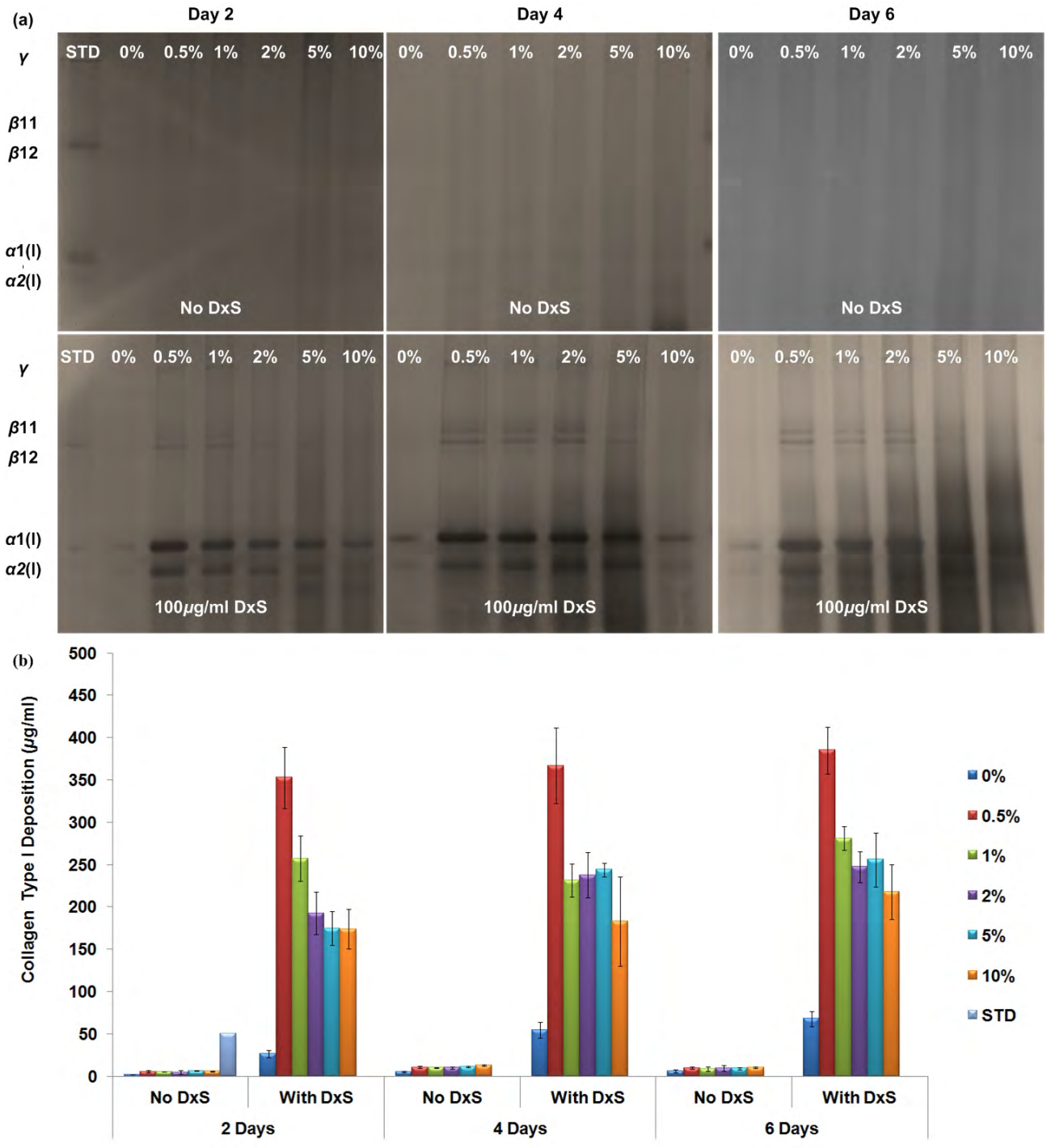

Supplementary Fig. S4 Gelatin zymography for WS1 human skin fibroblasts confirmed that the enhanced MMP-2 content as a function of increased FBS concentration.

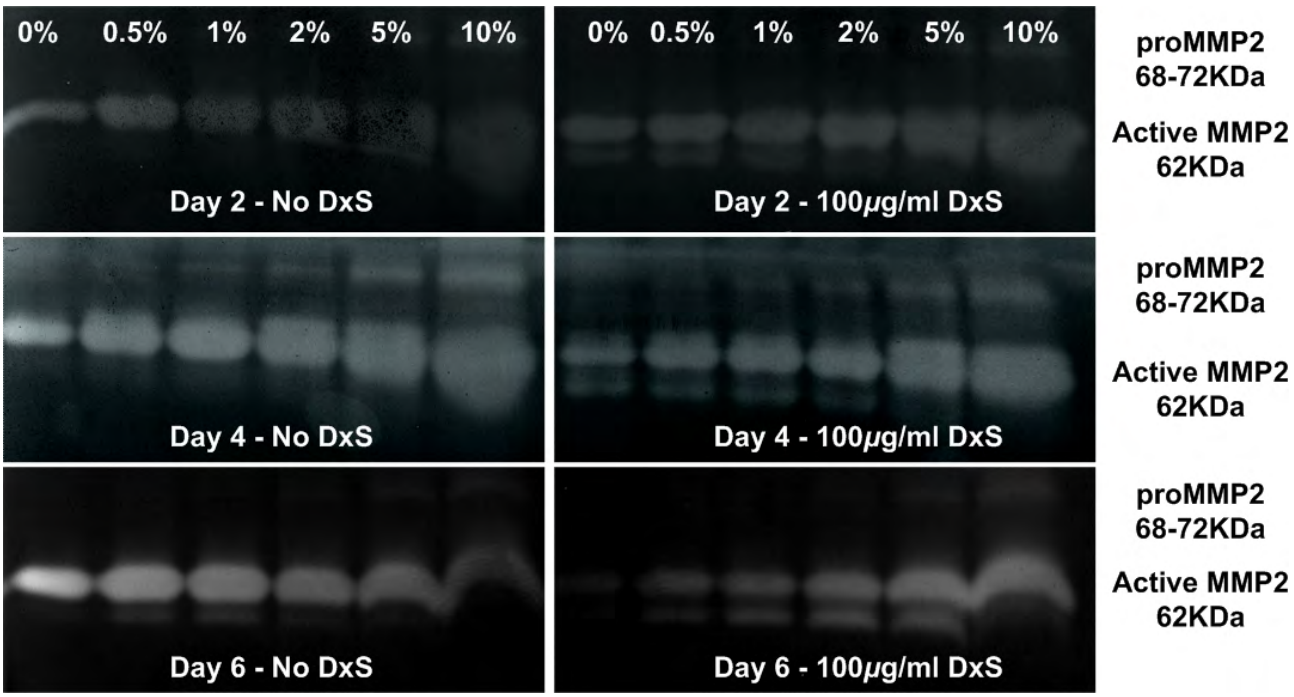

Supplementary Fig. S5 ICC analysis after 2 days of culture of WS1 human skin fibroblasts confirmed the higher collagen type I deposition in the presence of 100μg/ml 500kDa DxS. It also confirmed high deposition of collagen type I at low FBS concentrations. Fibronectin deposition was unchanged as a function of FBS concentration.

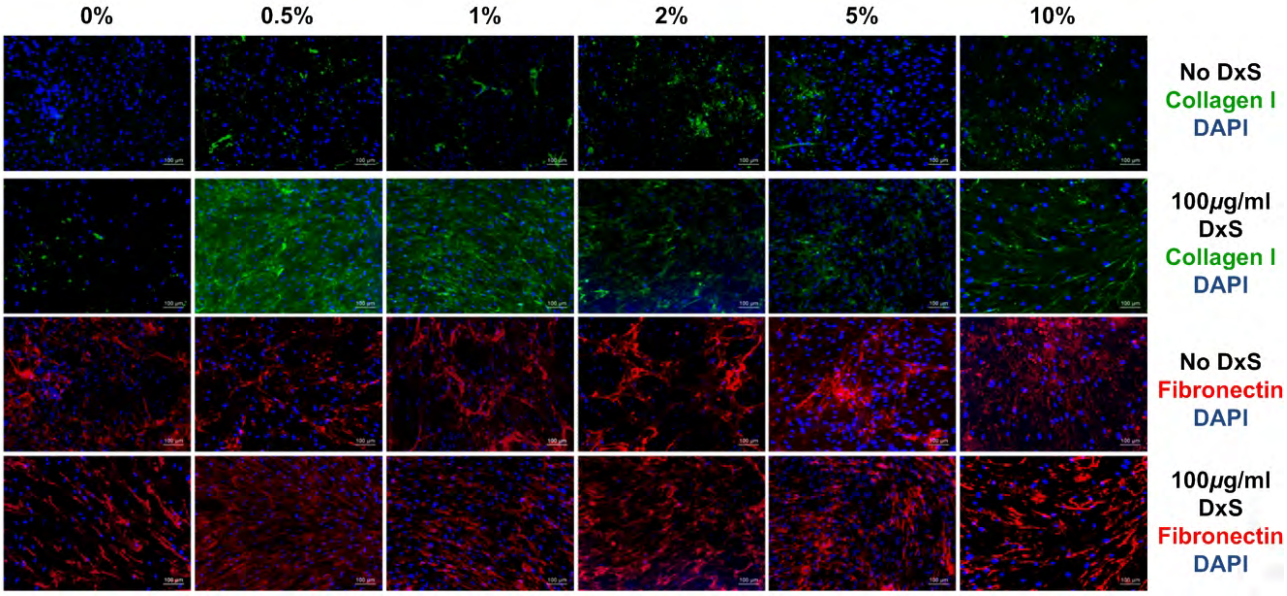

Supplementary Fig. S6 SDS-PAGE and complementary densitometric analysis showed that in the presence of 100μg/ml 500kDa DxS, WI38 fibroblasts deposit the highest (p<0.0001) amount of collagen type I in the presence of 0.5% HS after 2 days in culture. Specifically, an over 30-fold increase in collagen deposition was observed after 2 days in culture using 0.5% HS.

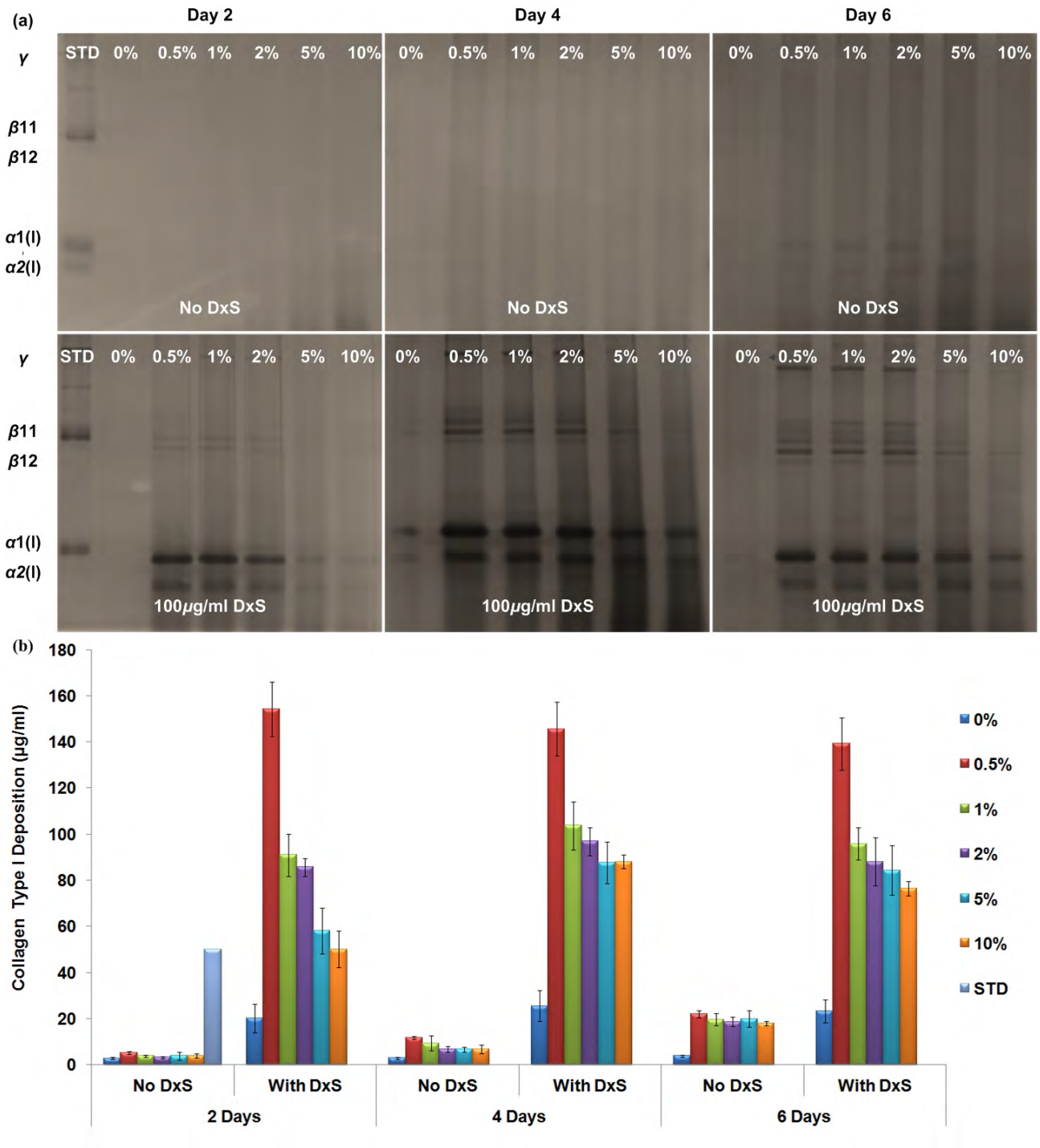

Supplementary Fig. S7 SDS-PAGE and complementary densitometric analysis showed that in the presence of 100μg/ml 500kDa DxS, WS1 fibroblasts deposit the highest amount of collagen type I in the presence of 0.5% HS after 2 days in culture (p<0.0001). Specifically, an over 80-fold increase in collagen deposition was observed after 2 days in culture using 0.5% HS.

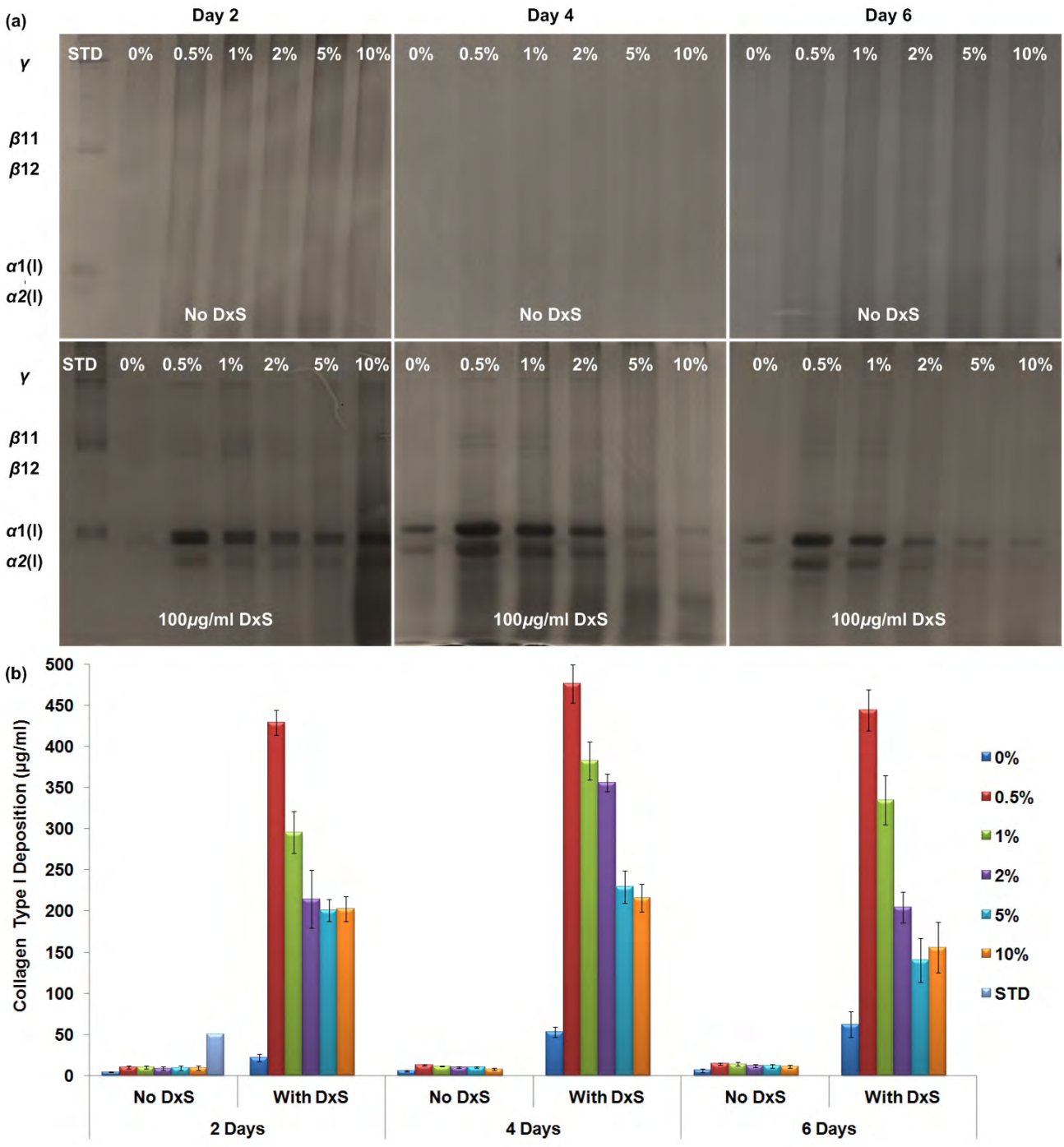

Supplementary Fig. S8 Gelatin zymography for WI38 (a) and WS1 (b) fibroblasts confirmed the enhanced MMP-2 content as a function of increased HS concentration.

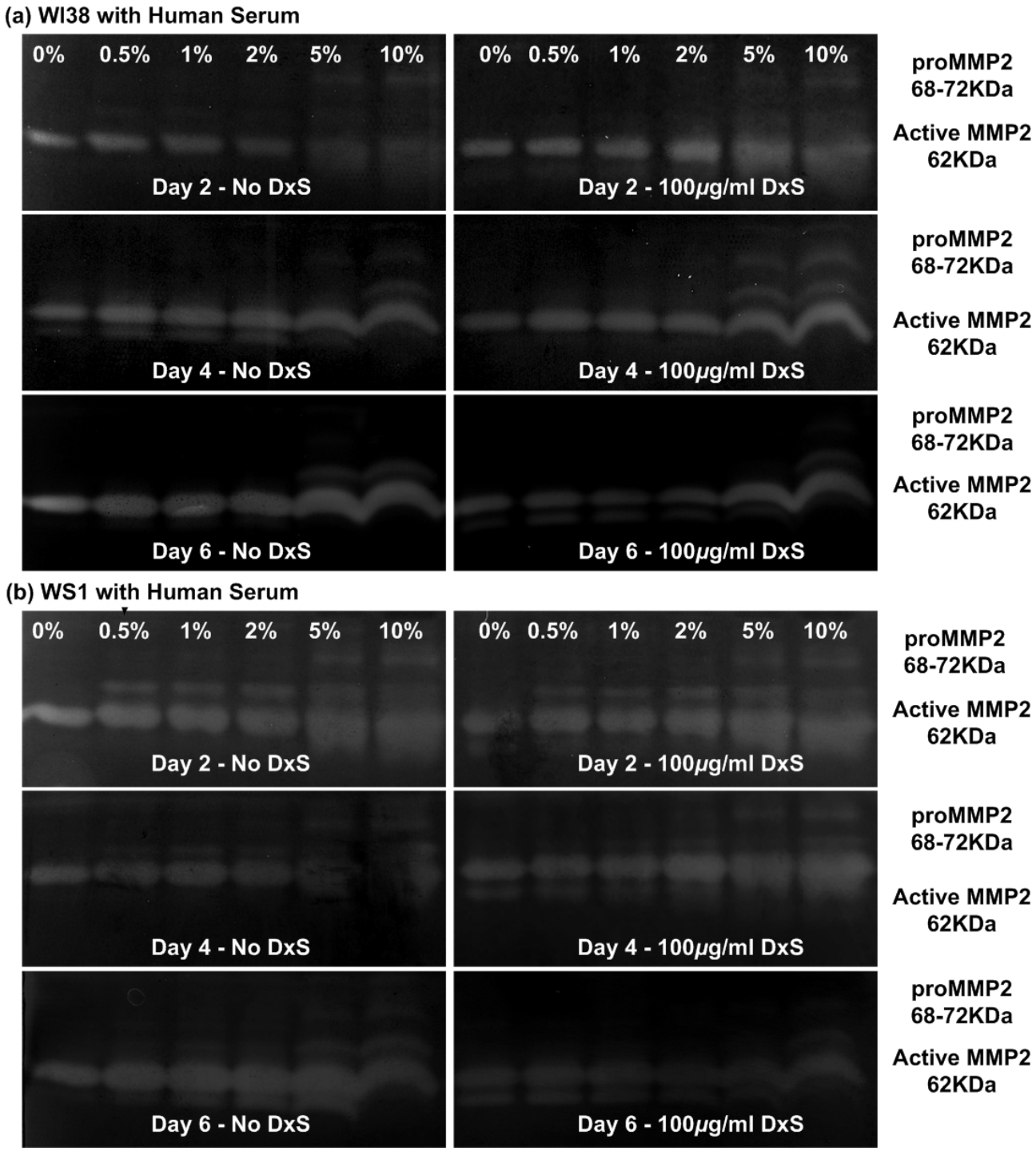

Supplementary Fig. S9 Dynamic light scattering (DLS) analysis for size (Z-ave, d.nm) of various negatively charged (DxS 500kDa and CR) and neutral (Ficoll™70, Ficoll™400) macromolecules revealed that negatively charged macromolecules were with higher hydrodynamic diameter than neutral counter part. CR exhibited the highest average hydrodynamic diameter than any other macromolecule.

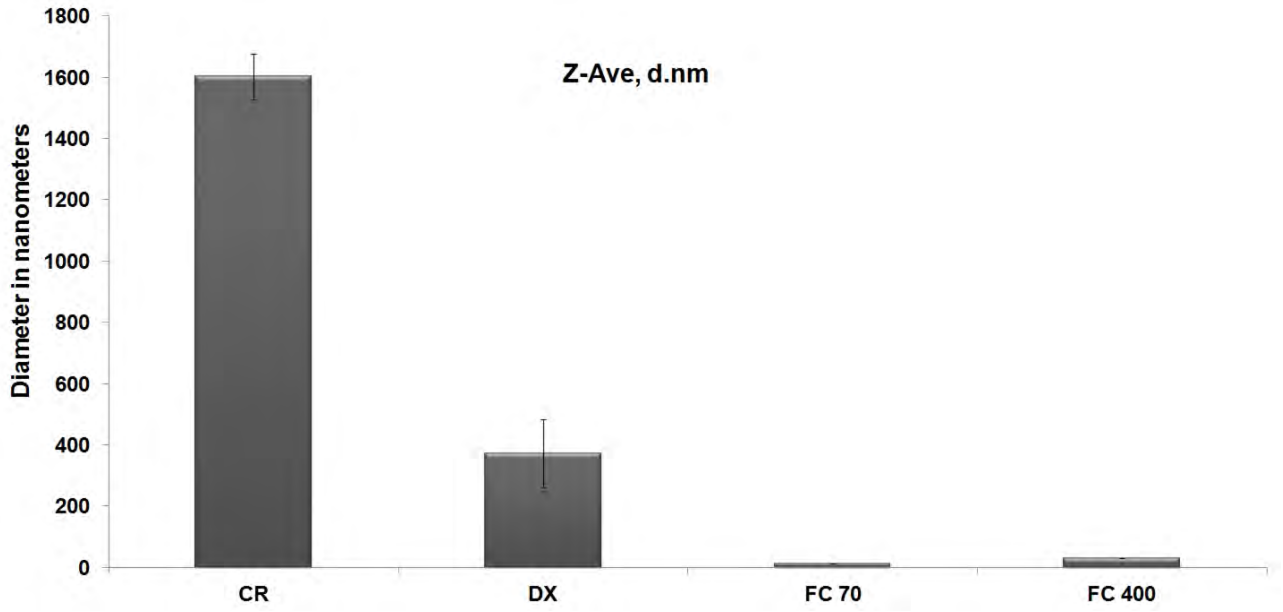

Supplementary Fig. S10a SDS-PAGE analysis of WS1 fibroblasts after 2 days in culture and at 10% FBS demonstrated that 75μg/ml CR induced maximum collagen type I deposition. Std: Symatese collagen type I (100μg/ml).

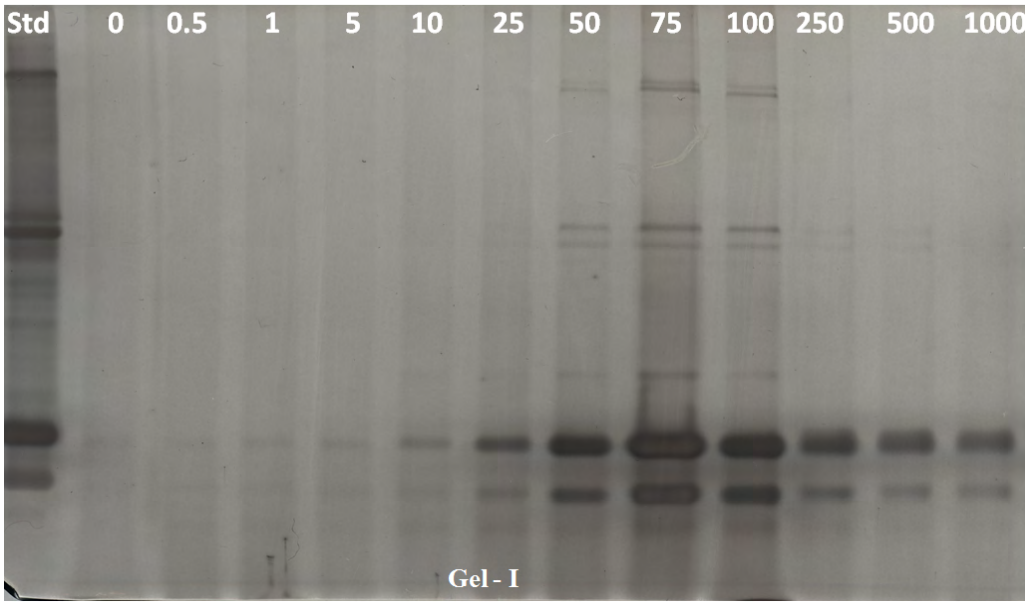

Supplementary Fig. S10b Complementary densitometric analysis demonstrated that 75μg/ml CR induce maximum collagen type I deposition (p<0.001) in WS1 fibroblast culture after 2 days and at 10% FBS. Lower than 75μg/ml CR concentrations do not create an effective excluding volume effect, whilst higher concentrations over-crowd the media prohibiting cleavage of procollagen and therefore reduce collagen type I deposition. Std: Symatese collagen type I (100μg/ml).

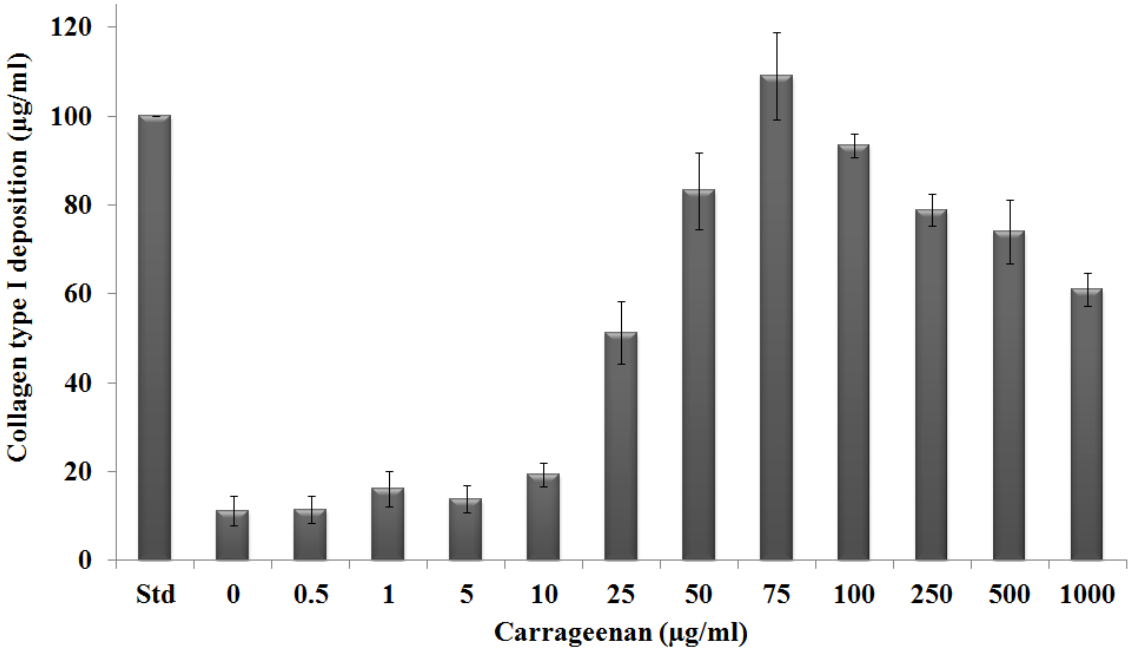

Supplementary Fig. S11 SDS-PAGE analysis of WI38 and WS1 fibroblasts after 2 days in culture and at 0.5% HS or FBS demonstrated that CR, the most polydispersed macromolecule, induced the highest collagen type I deposition.

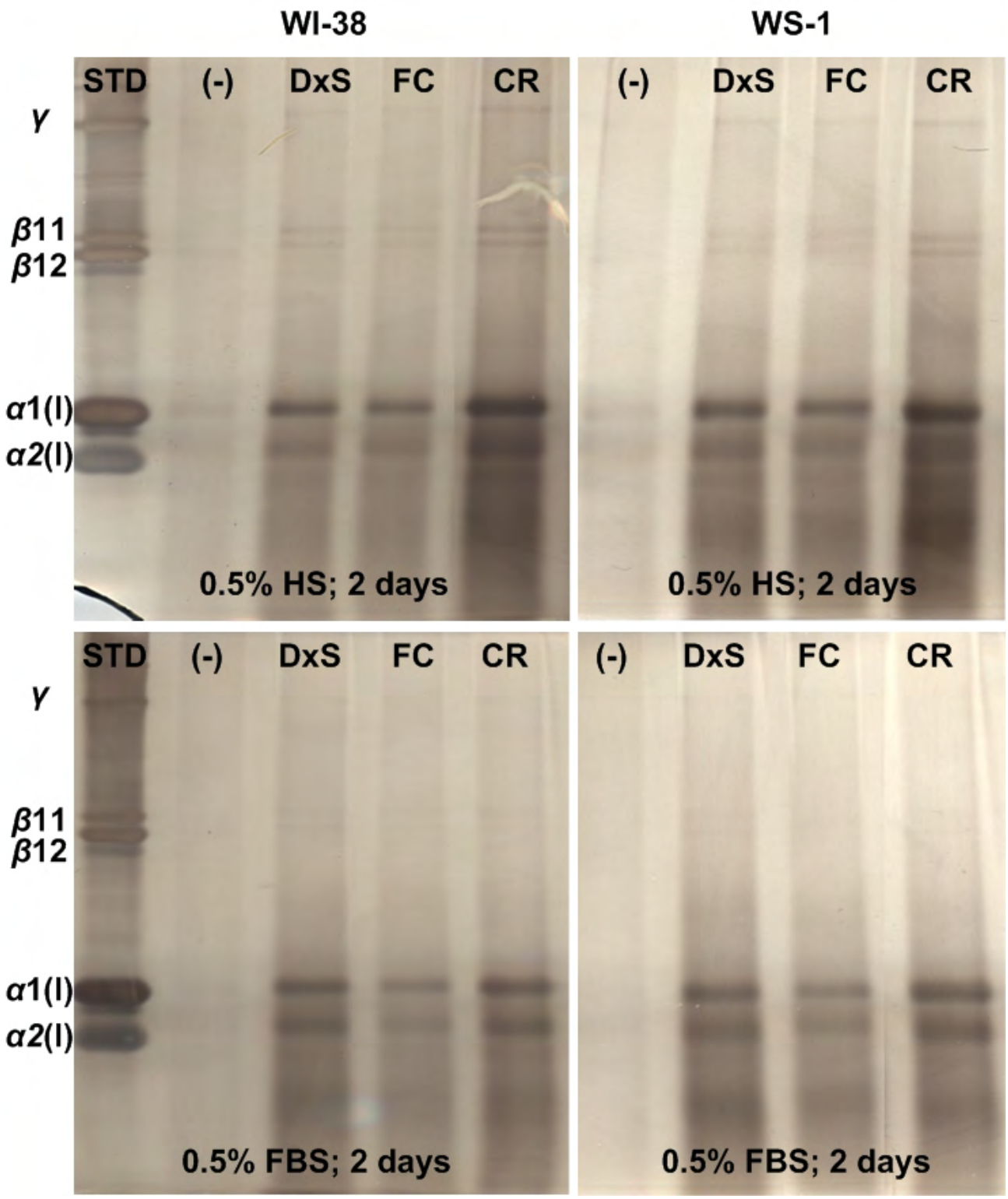

Supplementary Fig. S12 AlamarBlue® analysis revealed that WI-38 and WS-1 fibroblasts maintained their cellular metabolic activity after macromolecular crowding, 0.5% FBS or HS for all time points (2, 4 and 6 days).

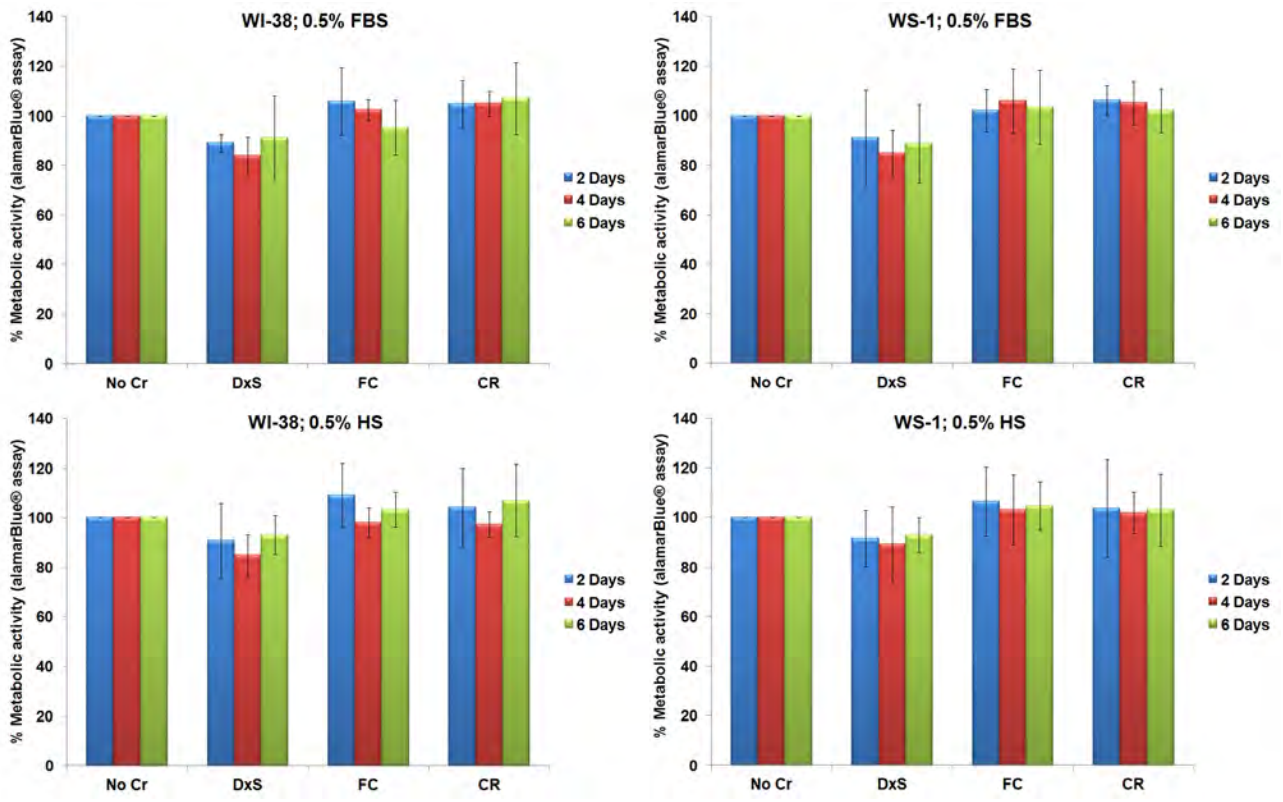

Supplementary Fig. S13 Live/Dead® assay for cell viability demonstrated that the various macromolecules did not affect cellular viability after macromolecular crowding, 0.5% FBS or HS for all time points (2, 4 and 6 days).

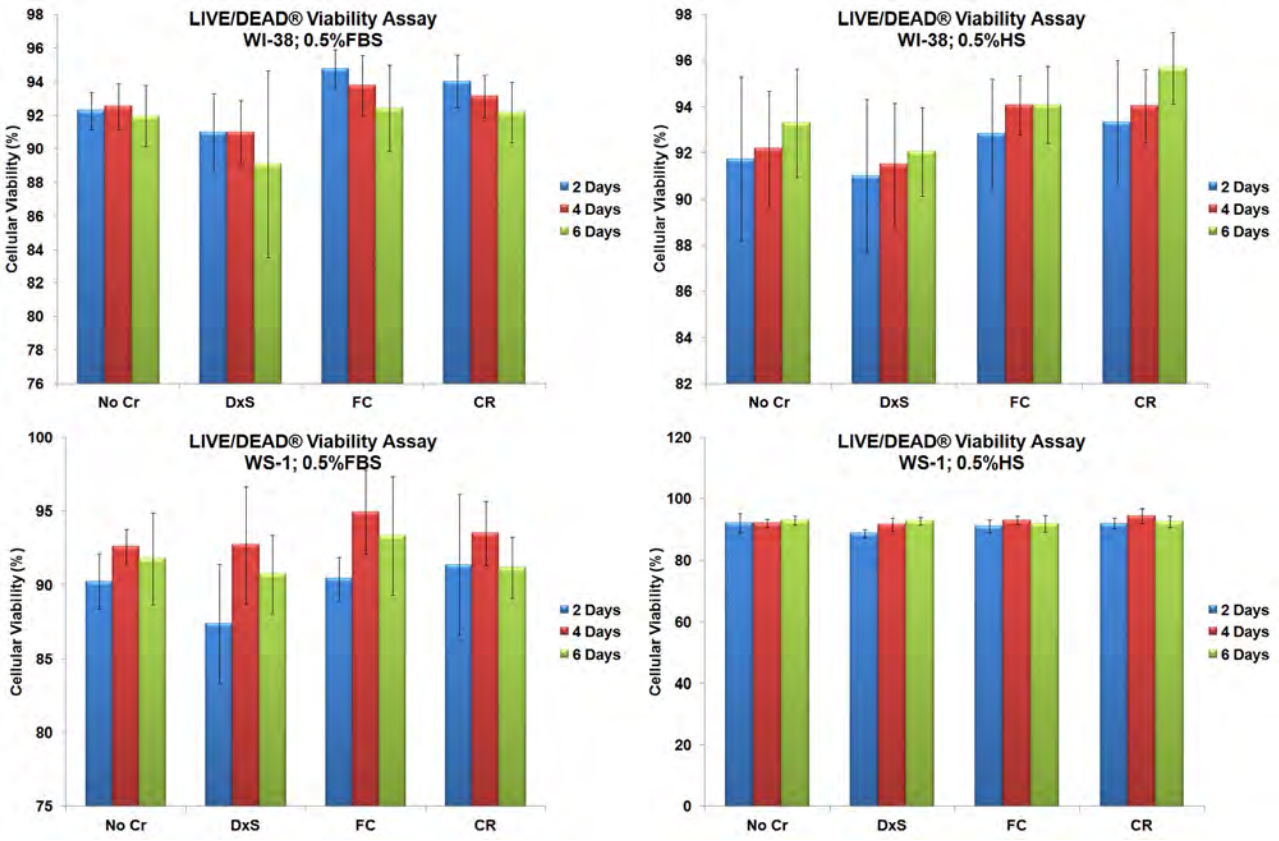

Supplementary Fig. S14 A 65% N-Isopropyl acrylamide + 35% N-tert-butyl acrylamide copolymer was found appropriate for cell attachment and detachment of intact fibroblast sheets. Due to high ECM deposition under MMC conditions, a slower detachment rate was observed using time-lapse analysis (a-f) and subsequent plotting of % detachment area against time (g).

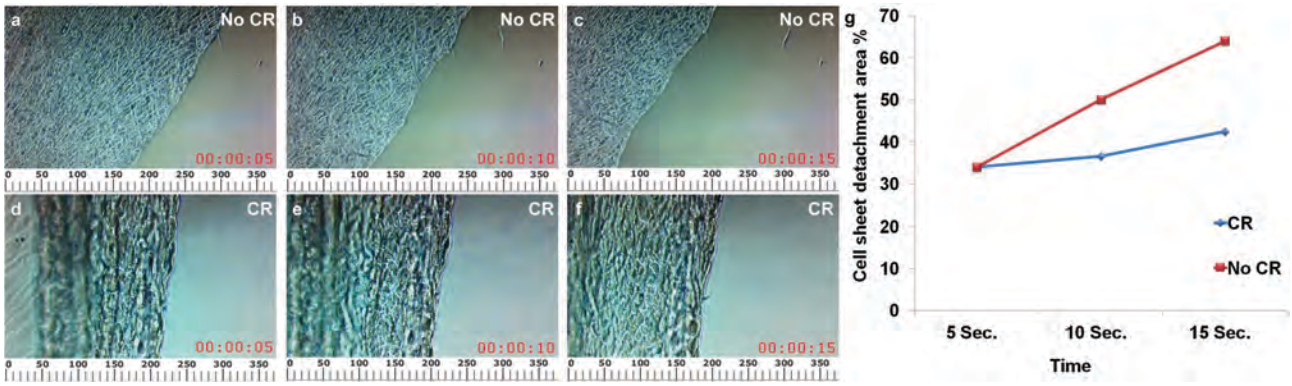

Supplementary Fig. S15 Masson`s Trichrome staining further corroborated the high/dense collagen matrix deposition under MMC condition (b).

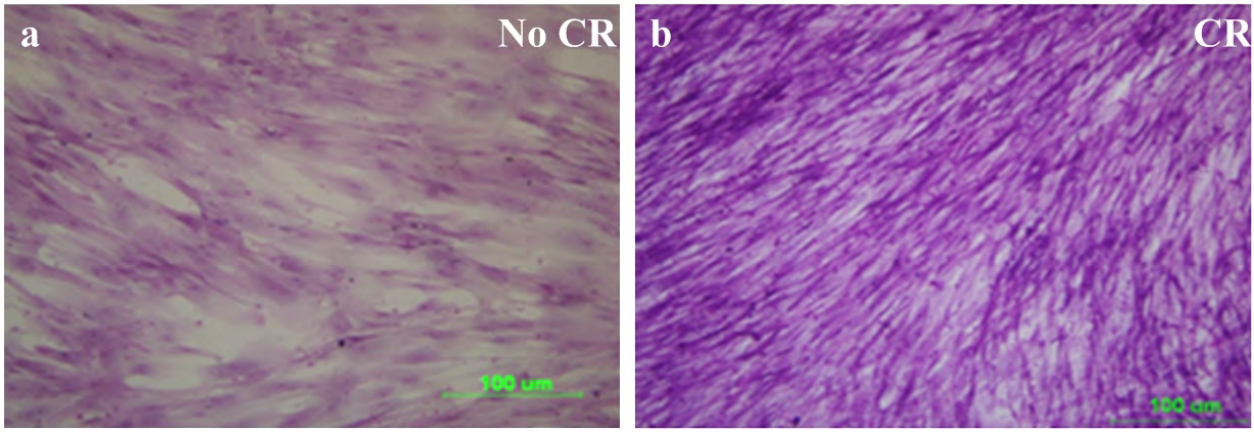

Supplementary Fig. S16 Representative (a-c) large (80 × 80μm^2), medium (25 × 25μm^2) and small (7 × 7μm^2) area AFM images of the cell sheet prepared without CR. Corresponding (d-f) large (90 × 90μm^2), medium (25 × 25μm^2) and small (8 × 8μm^2) area AFM images of the cell sheet prepared with CR. (g-i) large (90 × 90μm^2), medium (50 × 50μm^2) and small (5 × 5μm^2) area AFM images of the cell sheet prepared with CR from another location. The most striking difference between the no CR and CR images is the presence of a fibrous mesh in the intercellular region for cell sheets prepared under MMC conditions. Z scales: (a, g) 1μm; (b) 380nm; (c, f, i) 100nm; (d) 1.4μm; (e) 580nm; and (h) 220nm.

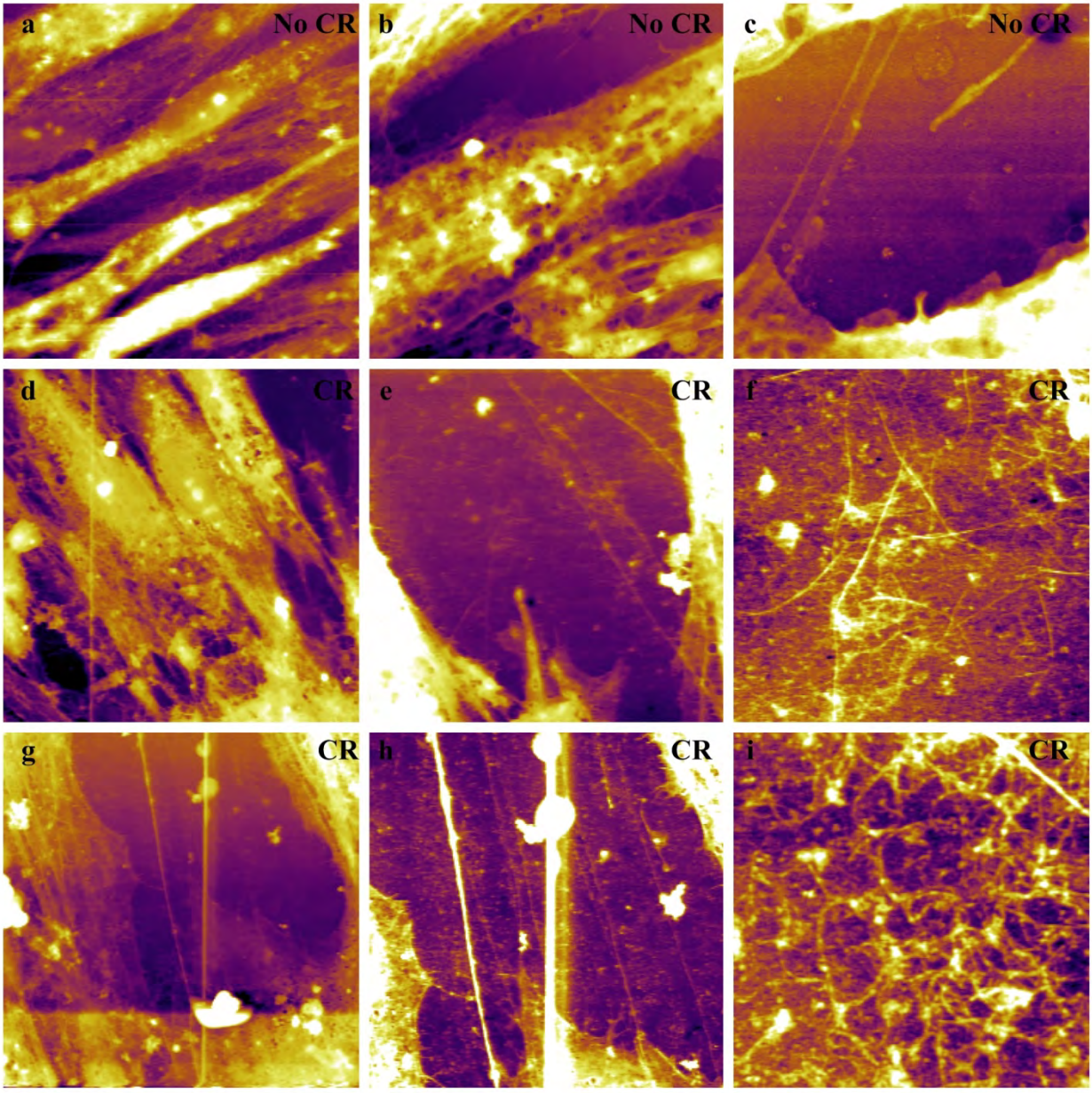

Supplementary Fig. S17 Representative (a-c) large (80 × 80μm^2), medium (20 × 20μm^2) and small (5 × 5μm^2) area AFM images of the cell sheet prepared without CR, which was cultured for 2 days. Corresponding (d-f) large (90 × 90μm^2), medium (15 × 15μm^2) and small (5 × 5μm^2) AFM area images of the cell sheet prepared with CR, which was cultured for 2 days. Thus, the presence of a fibrous mesh in the intercellular region for cell sheets prepared under MMC conditions is also apparent at this earlier time step. Z scales: (a,b,d) 600nm; (c) 20nm; (e) 300nm; and (f) 80nm.

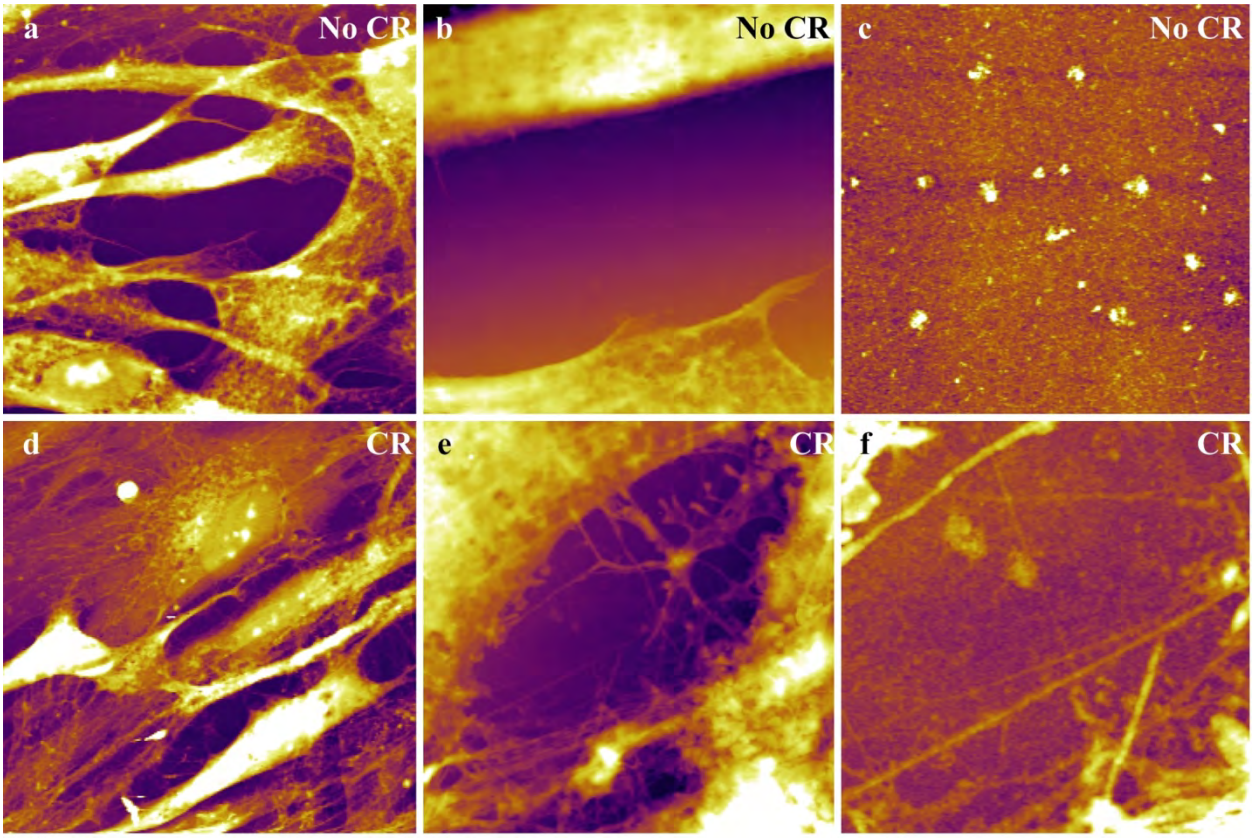

Supplementary Fig. S18 Proteomics validation using ICC (a) and complementary fluorescence intensity measurements (b) confirmed no significant change in ECM proteins (e.g. collagen type VII, elastin, fibrillin-1); cytoskeletal proteins (e.g. α-smooth muscle actin, epithelial keratin, tubulin); proteoglycans (e.g. aggrecan, biglycan); glycosaminoglycans (e.g. chondroitin sulphate, keratin sulphate, heparin sulphate); enzymes (e.g. transglutaminase-2); and cytokines (e.g. TEM-1 /CD248, IL-10).

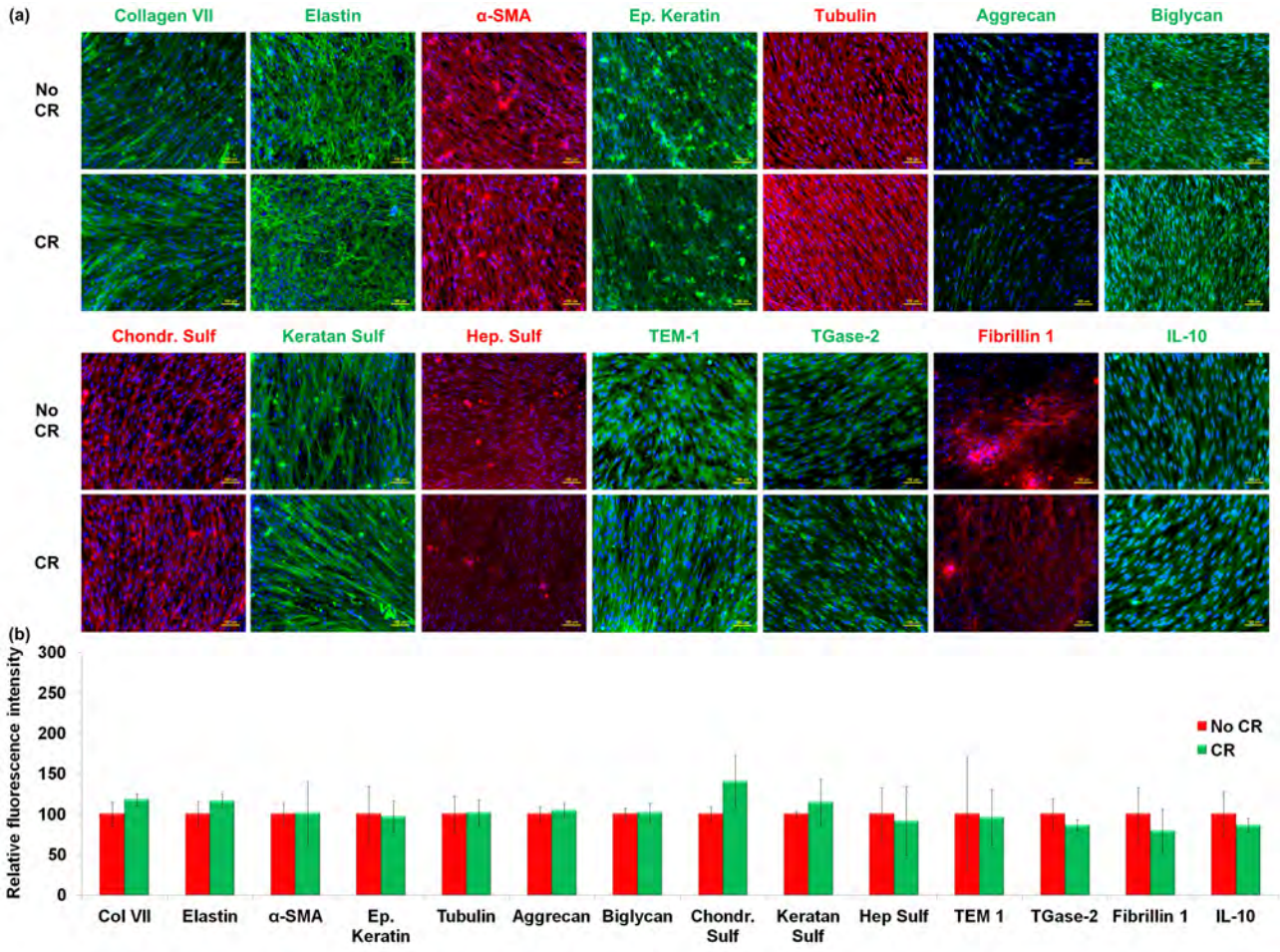

Supplementary Fig. S19 SDS-PAGE analysis of human tenocytes indicates that maximum collagen type I deposition was achieved after 6 days at 5% FBS in the presence of 75μg/ml CR.

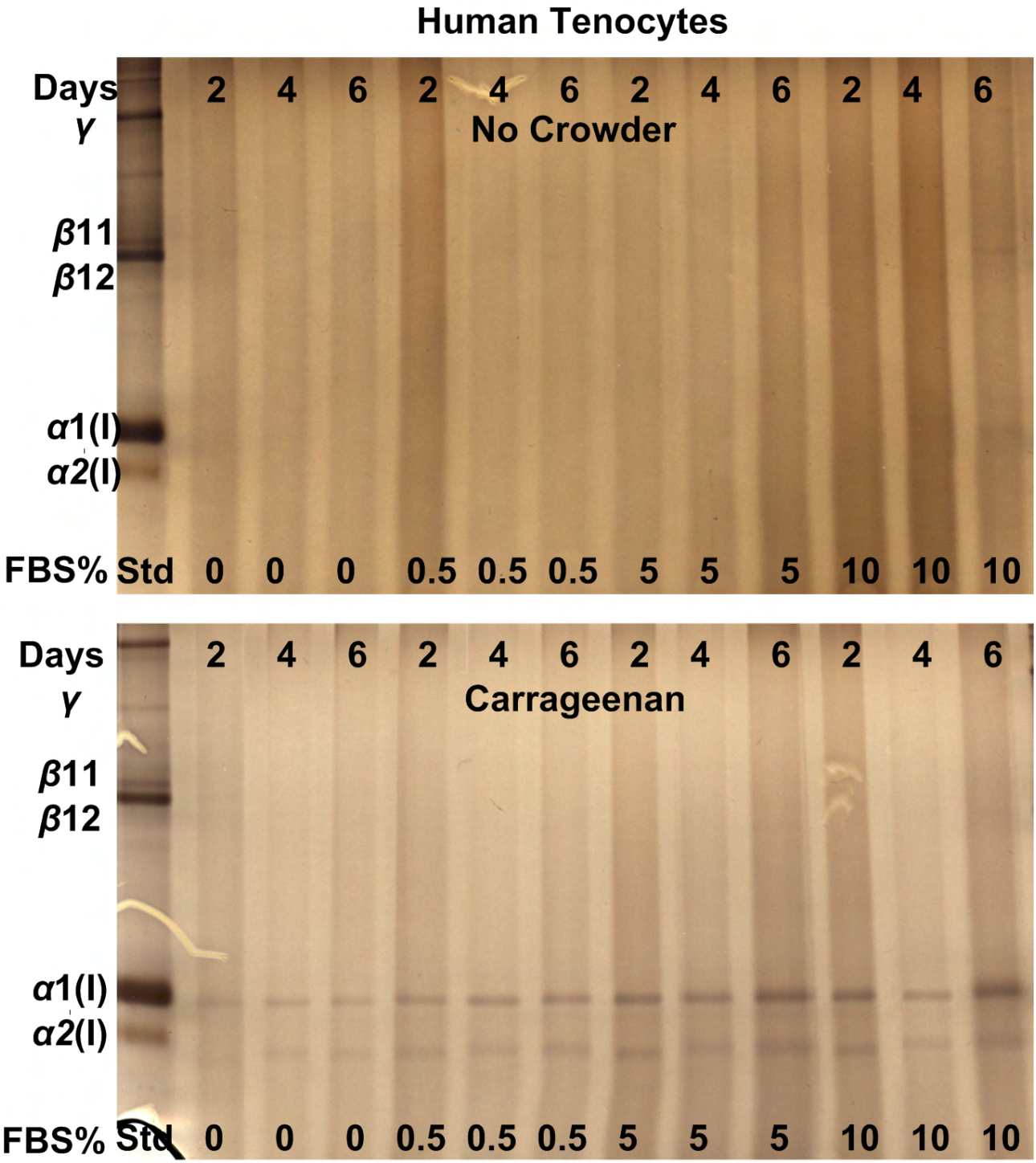

Supplementary Fig. S20 SDS-PAGE analysis of human osteoblasts indicates that maximum collagen type I deposition was achieved after 4 days at 5% FBS in the presence of 75μg/ml CR.

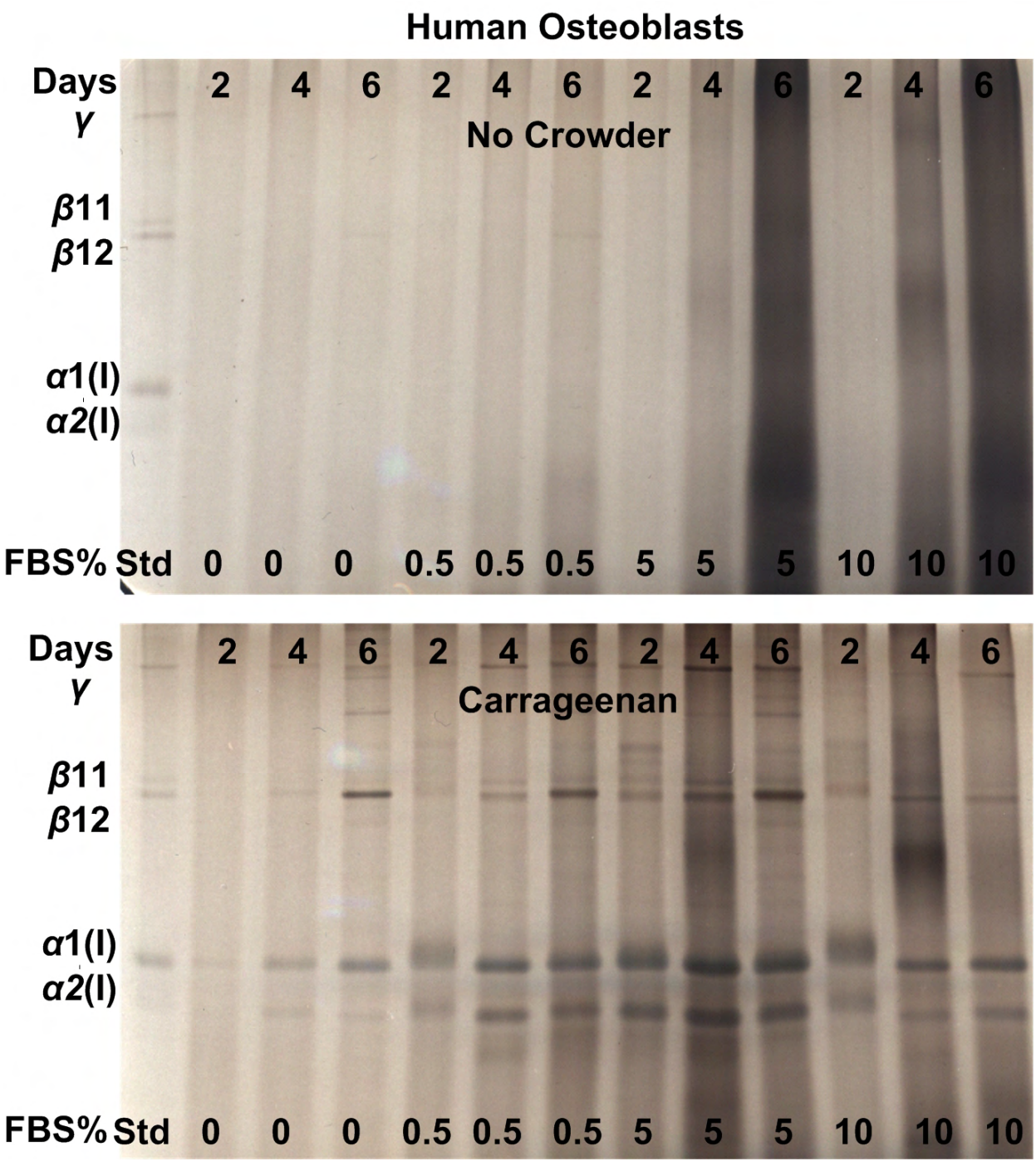

Supplementary Table S1: Mass spectrometry results of up-regulated (↑) and down-regulated (↓) proteins from human skin fibroblast in the presence of 0.5% HS under crowding condition with carrageenan (+CR) and non-crowding (-CR) conditions. ND indicates Not Detected.

1. Collagen and collagen related proteins in cell layer.

	Cell layer Proteins	Gene Symbol	PSMs	% Coverage	Ratio Cell +CR/-CR	log2 Fold change	↓↑
1	Collagen alpha-1(IV)	COL4A1	12	7.5	Cell-CR Only	ND	Cell -CR Only
2	Collagen alpha-1(XVIII)	COL18A1	6	5.8	Cell-CR Only	ND	Cell -CR Only
3	Collagen alpha-1(VI)	COL6A1	112	42.5	0.087455855	-3.5153	↓
4	Collagen, type VI, alpha 2	COL6A2	7	40.9	0.260755479	-1.93923	↓
5	Collagen alpha-2(VI)	COL6A2	22	24.5	0.271428571	-1.88136	↓
6	Collagen alpha-1(III)	COL3A1	11	6.6	0.490735542	-1.02698	↓
7	Collagen alpha-2(IV)	COL4A2	7	5.3	0.523833417	-0.93282	↓
8	Procollagen galactosyltransferase 1	GLT25D1	39	34.6	0.536113576	-0.89939	↓
9	Collagen alpha-1(I)	COL1A1	99	20.4	1.409865471	0.49556	↑
10	Collagen alpha-3(VI)	COL6A3	781	56.4	2.798348245	1.48458	↑
11	Collagen alpha-1(VIII)	COL8A1	2	3.9	2.938877043	1.55527	↑
12	Collagen alpha-1(XII)	COL12A1	577	55.2	3.24195122	1.69686	↑
13	Collagen alpha-1(XI)	COL11A1	4	3.1	3.488607595	1.80265	↑
14	Collagen alpha-2(I)	COL1A2	82	19.7	5.539296284	2.4697	↑
15	Collagen alpha-1(V)	COL5A1	56	13.8	6.617727026	2.72634	↑
16	Collagen triple helix repeat-containing protein	CTHRC1	17	33.3	6.697730956	2.74367	↑
17	Collagen alpha-2(V)	COL5A2	14	8.5	11.16728077	3.48121	↑
18	Collagen alpha-1(XVI)	COL16A1	1	2.3	Cell+CR Only	ND	Cell+CR Only
19	Collagen alpha-1(XIV)	COL14A1	9	6.8	Cell+CR Only	ND	Cell+CR Only
20	Collagen alpha-1(XVI)	COL16A1	1	2.3	Cell+CR Only	ND	Cell+CR Only
21	Collagen alpha-1(XIV)	COL14A1	9	6.8	Cell+CR Only	ND	Cell+CR Only
22	Procollagen C-endopeptidase enhancer 1	PCOLCE	23	46.5	Cell+CR Only	ND	Cell+CR Only

2. Fibronectin in cell layer.

	Cell layer Proteins	Gene Symbol	PSMs	% Coverage	Ratio Cell +CR/-CR	log2 Fold change	↓↑
1	Fibronectin type III domain-containing protein 3B	FNDC3B	7	6.6	Cell-CR Only	ND	Cell -CR Only
2	Fibronectin type-III domain-containing protein 3A	FNDC3A	1	4.2	Cell-CR Only	ND	Cell -CR Only
3	Fibronectin 1 (FN1)	FN1	1305	70.9	1.605209	0.682761	↑

3. Glycosaminoglycans (GAGs) and proteoglycans (PGs) in cell layer.

	Cell layer Proteins	Gene Symbol	PSMs	% Coverage	Ratio Cell +CR/-CR	log2 Fold change	↓↑
1	Basement membrane-specific heparan sulfate proteoglycan core protein	HSPG2	283	42.8	0.002009	-8.95951	↓
2	Chondroitin sulfate proteoglycan 4	CSPG4	73	28.1	0.480586	-1.05713	↓
3	Hyaluronan and proteoglycan link protein 1	HAPLN1	12	32.5	7.505923	2.90803	↑
4	Keratan sulphate	CHST1	ND	-	-	-	-
5	Aggrecan	ACAN	ND	-	-	ND	-
6	Biglycan	BGN	7	28.3	Cell-CR Only	ND	Cell-CR Only
7	Decorin	DCN	2	9.2	Cell-CR Only	ND	Cell-CR Only

4. Laminin in cell layer.

	Cell layer Proteins	Gene Symbol	PSMs	% Coverage	Ratio Media +CR/-CR	log2 Fold change	↓↑
1	Laminin subunit gamma-1	LAMC1	38	22.4	1.889876	0.91829	↑
2	Laminin subunit beta-1	LAMB1	62	29.6	2.452324	1.29415	↑
3	Laminin subunit beta-2	LAMB2	5	3.3	3.770306	1.91468	↑
4	Isoform 1 of Laminin subunit alpha-4	LAMA4	18	11.8	3.804566	1.92773	↑

5. Tubulins in cell layer.

	Cell layer Proteins	Gene Symbol	PSMs	% Coverage	Ratio Media +CR/-CR	log2 Fold change	↓↑
1	Tubulin beta-3 chain	TUBB3	23	72.4	0.096247655	-3.37710	↓
2	Tubulin beta-4 chain	TUBB4	13	76.8	0.3783420899	-1.40223	↓
3	Tubulin alpha-1C chain	TUBA1C	32	78.2	0.38150289	-1.39023	↓
4	Tubulin beta-8 chain	TUBB8	4	28.6	0.422291109	-1.243602	↓
5	Tubulin alpha-1A	TUBA1A	39	82.5	0.529806553	-0.916462	↓
6	Tubulin beta-2A chain	TUBB2A	18	82.9	1.150735294	0.202556	↑
7	Tubulin beta-2C chain	TUBB2C	6	82.9	1.442008487	0.528079	↑
8	Tubulin gamma-1 chain	TUBG1	2	6.7	Cell+CR Only	ND	Cell+CR Only

6. Other ECM and cytoskeleton proteins.

	Cell layer Proteins	Gene Symbol	PSMs	% Coverage	Ratio Media +CR/-CR	log2 Fold change	↓↑
1	Elastin	ELN	ND	-	-	-	-
2	Actin, aortic smooth muscle	ACTA2	7	74.5	0.229640981	-2.12254	↓
3	Isoform 1 of Keratin	KRT13	14	32.6	Cell-CR Only	ND	Cell-CR Only
4	Keratin, type I cytoskeletal 18	KRT18	7	10.7	Cell-CR Only	ND	Cell-CR Only
5	Keratin, type II cytoskeletal 3	KRT3	5	17	0.192553749	-2.376666	↓
6	Fibrillin-1	FBN1	170	29.3	5.459476707	2.4487626	↑

7. Interleukins and enzymes in cell layer.

	Cell layer Proteins	Gene Symbol	PSMs	% Coverage	Ratio Media +CR/-CR	log2 Fold change	↓↑
1	Isoform 1 of Interleukin enhancer-binding factor 3	ILF3	49	28.5	0.182498	-2.45405	↓
2	Interleukin enhancer-binding factor 2	ILF2	40	54.1	0.861507	-0.21507	↓
3	Isoform 1 of Interleukin-36 gamma	IL36G	4	44.8	Cell+CR Only	ND	Cell+CR Only
4	Interleukin-10	IL10	ND	-	-	-	-
5	Isoform 1 of Endosialin (TEM1)	CD248	20	22.7	0.016694547	-5.90447	↓
6	Lysyl oxidase homolog 2	LOXL2	19	14.6	0.719667944	-0.47459	↓
7	Transglutaminase 2	TGM2	ND	-	-	-	-

8. Matrix metalloproteinases (MMPs) and tissue inhibitor metalloproteinases (TIMPs) in cell layer.

	Cell layer Proteins	Gene Symbol	PSMs	% Coverage	Ratio Cell +CR/-CR	log2 Fold change	↓↑
1	Matrix metalloproteinase	MMP14	26	21.1	2.001448226	1.0010442	↑
2	72 KDa type IV collagenase	MMP2	44	46.5	2.390903503	1.2575559	↑
3	Interstitial collagenase	MMP1	50	43.5	Cell+CR Only	ND	Cell+CR Only
4	Metalloproteinase inhibitor 1	TIMP1	15	76.9	5.409454061	ND	↑
5	Metalloproteinase inhibitor 3	TIMP3	2	11.4	Cell+CR Only	ND	Cell+CR Only
6	Metalloproteinase inhibitor 2	TIMP2	4	41.3	Cell+CR Only	ND	Cell+CR Only

Table S2a: Cell layer proteomics analysis with CR (+CR) and without CR (-CR); (↑) indicates upregulation, whilst (↓) indicates down regulation; ND indicates Not Detected.

			Protein Accession No	Description	InterProphet Probability	Peptide Spectrum Matches (PSMs)	Unique peptides	% Coverage	Cells+CR / Cells-CR	(↑) / (↓)
Molecular Functions	**1. Antioxidant activity**	**1**	sp|P35354|PGH2_HUMAN	Prostaglandin G/H synthase 2	1.00	7	7	15.4%	**ND Cells - CR**	↑
	2. Catalytic activity	**1**	sp|Q969Z0|TBRG4_HUMAN	Protein TBRG4 / Transforming growth factor beta regulator 4	1.00	8	6	16.3%	**ND Cells +CR**	↓
		2	sp|P50570-2|DYN2_HUMAN	Dynamin-2	1.00	6	7	10.3%	**ND Cells - CR**	↑
		3	sp|P20930|FILA_HUMAN	Filaggrin	1.00	8	5	5.7%	23.37	↑
		4	sp|P03956|MMP1_HUMAN	Interstitial collagenase (MMP1)	1.00	49	17	43.5%	**ND Cells - CR**	↑
	3. DNA binding	**1**	sp|P09429|HMGB1_HUMAN	High mobility group protein B1	1.00	10	8	35.3%	**ND Cells +CR**	↓
		2	sp|P52630|STAT2	Signal transducer and	1.00	12	10	16.1%	0.003	↓

			_HUMAN	activator of transcription 2						
		3	sp|P42704|LPPRC_HUMAN	Leucine-rich PPR motif-containing protein, mitochondrial	1.00	85	50	42.8%	0.018	↓
	4. Enzyme regulator activity	**1**	sp|Q9Y3P9|RBGP1_HUMAN	Rab GTPase-activating protein 1	1.00	7	6	6.2%	**ND Cells +CR**	↓
		2	sp|Q96P63|SPB12_HUMAN	Serpin B12	1.00	9	7	33.6%	**ND Cells - CR**	↑
		3	sp|P01040|CYTA_HUMAN	Cystatin-A	1.00	14	7	83.7%	**ND Cells - CR**	↑
		4	sp|Q15113|PCOC1_HUMAN	Procollagen C-endopeptidase enhancer 1	1.00	23	11	46.5%	**ND Cells - CR**	↑
	5. Metal ion binding	**1**	sp|Q14517|FAT1_HUMAN	Protocadherin Fat 1	1.00	17	14	3.9%	**ND Cells +CR**	↓
		2	sp|Q7L5N7|PCAT2_HUMAN	Lysophosphatidylcholine acyltransferase 2	1.00	6	5	18.4%	**ND Cells +CR**	↓
		3	sp|P35354|PGH2_HUMAN	Prostaglandin G/H synthase 2	1.00	7	7	15.4%	**ND Cells - CR**	↑
		4	sp|Q86YZ3|HORN_HUMAN	Hornerin	1.00	21	11	20.2%	**ND Cells - CR**	↑
	6. Motor	**1**	sp|Q14789|GOGB	Golgin subfamily B	1.00	42	40	17%	**ND Cells**	↓

	activity		1_HUMAN	member 1					**+CR**	
		2	sp|Q9UM54-1|MYO6_HUMAN	Unconventional myosin-VI	1.00	11	11	13.5%	**ND Cells +CR**	↓
		3	sp|O00159-3|MYO1C_HUMAN	Unconventional myosin-Ic	1.00	87	37	45.2%	0.021	↓
		4	sp|P63167|DYL1_HUMAN	Dynein light chain 1, cytoplasmic	1.00	19	8	65.2%	0.026	↓
	7. Nucleotide Binding	**1**	sp|Q14699|RFTN1_HUMAN	Raftlin	1.00	9	5	21.5%	**ND Cells +CR**	↓
		2	sp|P08237|K6PF_HUMAN	6-phosphofructokinase, muscle type	1.00	8	11	20%	**ND Cells +CR**	↓
		3	sp|P29323-2|EPHB2_HUMAN	Ephrin type-B receptor 2	1.00	7	9	13.4%	**ND Cells - CR**	↑
		4	sp|Q9UBQ7|GRHPR_HUMAN	Glyoxylate reductase/hydroxypyruvate reductase	1.00	8	7	36.3%	**ND Cells - CR**	↑
	8. Protein binding	**1**	sp|Q9NR99|MXRA5_HUMAN	Matrix-remodeling-associated protein 5	1.00	16	8	3.9%	**ND Cells - CR**	↑
		2	sp|Q5VW36|FOCAD_HUMAN	Focadhesin	1.00	8	6	5.6%	**ND Cells +CR**	↓

		3	sp|Q9HB71|CYBP_HUMAN	Calcyclin-binding protein	1.00	7	6	52.4%	**ND Cells +CR**	↓
		4	sp|Q9UHA4|LTOR3_HUMAN	Ragulator complex protein LAMTOR3	1.00	8	5	62.1%	**ND Cells +CR**	↓
		5	sp|P02745|C1QA_HUMAN	Complement C1q subcomponent subunit A	1.00	7	5	29%	**ND Cells - CR**	↑
		6	sp|P04003|C4BPA_HUMAN	C4b-binding protein alpha chain	1.00	9	7	16.9%	**ND Cells - CR**	↑
		7	sp|Q05707-2|COEA1_HUMAN	Collagen alpha-1(XIV) chain	1.00	9	6	6.8%	**ND Cells - CR**	↑
		8	sp|P02747|C1QC_HUMAN	Complement C1q subcomponent subunit C	1.00	10	5	25.3%	**ND Cells - CR**	↑
	9. Receptor activity	**1**	sp|Q53EP0|FND3B_HUMAN	Fibronectin type III domain-containing protein 3B	1.00	8	5	6.6%	**ND Cells +CR**	↓
		2	sp|P27487|DPP4_HUMAN	Dipeptidyl peptidase 4	1.00	6	7	9.5%	**ND Cells +CR**	↓
		3	sp|Q08AM6|VAC14_HUMAN	Protein VAC14 homolog	1.00	9	7	11.8%	0.014	↓
		4	sp|P18084|ITB5_HUMAN	Integrin beta-5	1.00	21	17	29.8%	0.026	↓
	10. RNA	**1**	sp|Q9Y2X3|NOP	Nucleolar protein 58	1.00	12	9	22.7%	**ND Cells**	↓

	binding		58_HUMAN						**+CR**	
		2	sp|Q9ULC4-2|MCTS1_HUMAN	Malignant T-cell-amplified sequence 1	1.00	6	5	39.1%	**ND Cells +CR**	↓
		3	sp|O14980|XPO1_HUMAN	Exportin-1	1.00	42	22	28.4%	0.014	↓
		4	sp|Q7L2H7|EIF3M_HUMAN	Eukaryotic translation initiation factor 3 subunit M	1.00	12	9	35%	36.1%	↑
	11. Signal transducer activity	**1**	sp|P52630|STAT2_HUMAN	Signal transducer and activator of transcription 2	1.00	12	10	16.1%	0.003	↓
		2	sp|O75533|SF3B1_HUMAN	Splicing factor 3B subunit 1	1.00	28	16	17.8%	0.011	↓
		3	sp|P29317|EPHA2_HUMAN	Ephrin type-A receptor 2	1.00	11	11	13.6%	0.012	↓
	12. Structural Molecule activity	**1**	sp|P02462-2|CO4A1_HUMAN	Collagen alpha-1(IV) chain	1.00	12	7	7.5%	**ND Cells +CR**	↓
		2	sp|O95292|VAPB_HUMAN	Vesicle-associated membrane protein-associated protein B/C	1.00	8	6	25.1%	**ND Cells +CR**	↓
		3	sp|P23142|FBLN1_HUMAN	Fibulin-1	1.00	10	12	26.3%	0.014	↓

		4	sp|P53621|COPA_HUMAN	Coatomer subunit alpha	1.00	116	53	51.8%	0.024	↓
	13.Trabscription regulator activity	N/A	N/A							
	14.Translation regulator activity	N/A	N/A							
	15. Transporter activity	**1**	sp|Q9UIA9|XPO7_HUMAN	Exportin-7	1.00	6	6	7.5%	**ND Cells +CR**	↓
		2	sp|O14980|XPO1_HUMAN	Exportin-1	1.00	42	22	28.4%	0.015	↓
		3	sp|Q14974|IMB1_HUMAN	Importin subunit beta-1	1.00	75	33	51.3%	0.019	↓
		4	sp|P04114|APOB_HUMAN	Apolipoprotein B-100	1.00	1000	170	47.5%	1393	↑
Cellular Components	**1. Cell Surface**	**1**	sp|Q14517|FAT1_HUMAN	Protocadherin Fat 1	1.00	17	14	3.9%	**ND Cells +CR**	↓
		2	sp|P09429|HMGB1_HUMAN	High mobility group protein B1	1.00	10	8	35.3%	**ND Cells +CR**	↓
		3	sp|P21810|PGS1_HUMAN	Biglycan	1.00	7	7	28.3%	**ND Cells +CR**	↓

		4	sp|P27487|DPP4_HUMAN	Dipeptidyl peptidase 4	1.00	6	7	9.5%	**ND Cells +CR**	↓
	2. Chromosome	**1**	sp|P09429|HMGB1_HUMAN	High mobility group protein B1	1.00	10	8	35.3%	**ND Cells +CR**	↓
		2	sp|O14980|XPO1_HUMAN	Exportin-1	1.00	42	22	28.4%	0.015	↓
		3	sp|P42704|LPPRC_HUMAN	Leucine-rich PPR motif-containing protein	1.00	81	50	42.8%	0.018	↓
		4	sp|P60228|EIF3E_HUMAN	Eukaryotic translation initiation factor 3 subunit E	1.00	24	16	44.3%	35.8	↑
	3. Cytoplasm	**1**	sp|Q99426|TBCB_HUMAN	Tubulin-folding cofactor B	1.00	9	8	44.3%	**ND Cells +CR**	↓
		2	sp|Q6UB35|C1TM_HUMAN	Monofunctional C1-tetrahydrofolate synthase	1.00	6	6	7.9%	**ND Cells +CR**	↓
		3	sp|P48147|PPCE_HUMAN	Prolyl endopeptidase	1.00	22	17	36.5%	0.027	↓
		4	sp|Q9UBQ7|GRHPR_HUMAN	Glyoxylate reductase/hydroxypyruvate reductase	1.00	8	7	36.3%	**ND Cells - CR**	↑
		5	sp|P01009|A1AT_HUMAN	Alpha-1-antitrypsin	1.00	19	11	40.7%	**ND Cells - CR**	↑
	4.	**1**	sp|Q08379|GOGA	Golgin subfamily A	1.00	7	5	5.3%	**ND Cells**	↓

	Cytoskeleton		2_HUMAN	member 2					**+CR**	
		2	sp|P50552|VASP_HUMAN	Vasodilator-stimulated phosphoprotein	1.00	7	4	12.4%	**ND Cells +CR**	↓
		3	sp|Q9Y3A5|SBDS_HUMAN	Ribosome maturation protein SBDS	1.00	7	5	32.8%	**ND Cells +CR**	↓
		4	sp|Q86YZ3|HORN_HUMAN	Hornerin	1.00	21	11	20.2%	**ND Cells - CR**	↑
	5. Cytosol	**1**	sp|P08237|K6PF_HUMAN	6-phosphofructokinase, muscle type	1.00	8	11	20%	**ND Cells +CR**	↓
		2	sp|P61513|RL37A_HUMAN	60S ribosomal protein L37a	1.00	8	6	66.3%	**ND Cells +CR**	↓
		3	sp|Q9HAB8|PPCS_HUMAN	Phosphopantothenate--cysteine ligase	1.00	6	5	12.5%	**ND Cells +CR**	↓
		4	sp|P19784|CSK22_HUMAN	Casein kinase II subunit alpha'	1.00	6	5	21.1%	**ND Cells - CR**	↑
		1	sp|Q9H223|EHD4_HUMAN	EH domain-containing protein 4	1.00	6	9	17.6%	**ND Cells +CR**	↓
		2	sp|Q92575|UBXN4_HUMAN	UBX domain-containing protein 4	1.00	6	4	14.1%	**ND Cells +CR**	↓
		3	sp|P51571|SSRD_HUMAN	Translocon-associated protein subunit delta	1.00	20	6	37%	0.026	↓
	7. Endosome	**1**	sp|Q9UHA4|LTOR3_HUMAN	Ragulator complex protein LAMTOR3	1.00	8	5	62.1%	**ND Cells +CR**	↓

		2	sp|Q9H223|EHD4_HUMAN	EH domain-containing protein 4	1.00	6	9	17.6%	**ND Cells +CR**	↓
		3	sp|Q08AM6|VAC14_HUMAN	Protein VAC14 homolog	1.00	9	7	11.8%	0.014	↓
		4	sp|P04114|APOB_HUMAN	Apolipoprotein B-100	1.00	1000	170	47.5%	1393	↑
	8. Extracellular	**1**	sp|P02462-2|CO4A1_HUMAN	Collagen alpha-1(IV) chain	1.00	12	7	7.5%	**ND Cells +CR**	↓
		2	sp|Q9NR99|MXRA5_HUMAN	Matrix-remodeling-associated protein 5	1.00	16	8	3.9%	**ND Cells - CR**	↑
		3	sp|P09429|HMGB1_HUMAN	High mobility group protein B1	1.00	10	8	35.3%	**ND Cells +CR**	↓
		4	sp|P02808|STAT_HUMAN	Statherin	1.00	8	2	54.8%	**ND Cells +CR**	↓
		5	sp|P21810|PGS1_HUMAN	Biglycan	1.00	7	7	28.3%	**ND Cells +CR**	↓
		6	sp|P27487|DPP4_HUMAN	Dipeptidyl peptidase 4	1.00	6	7	9.5%	**ND Cells +CR**	↓
		7	sp|P98160|PGBM_HUMAN	Basement membrane-specific heparan sulfate proteoglycan core protein	1.00	277	110	42.8%	0.006	↓
		8	sp|P23142|FBLN1	Fibulin-1	1.00	10	12	26.3%	0.014	↓

			_HUMAN							
		9	sp|P35442|TSP2_HUMAN	Thrombospondin-2	1.00	28	17	19.3%	35.9	↑
		10	sp|P01859|IGHG2_HUMAN	Ig gamma-2 chain C region	1.00	11	9	41.7%	48.2	↑
		11	sp|P04114|APOB_HUMAN	Apolipoprotein B-100	1.00	1000	170	47.5%	1393	↑
		12	sp|P01024|CO3_HUMAN	Complement C3	1.00	48	29	27.6	1554	↑
		13	sp|P00738|HPT_HUMAN	Haptoglobin	1.00	8	10	39.5%	**ND Cells - CR**	↑
		14	sp|P02745|C1QA_HUMAN	Complement C1q subcomponent subunit A	1.00	7	5	29%	**ND Cells - CR**	↑
		15	sp|P01860|IGHG3_HUMAN	Ig gamma-3 chain C region	1.00	8	10	34.7%	**ND Cells - CR**	↑
		16	sp|P08519|APOA_HUMAN	Apolipoprotein(a)	1.00	9	5	25.9%	**ND Cells - CR**	↑
		17	sp|P04003|C4BPA_HUMAN	C4b-binding protein alpha chain	1.00	9	7	16.9%	**ND Cells - CR**	↑
		18	sp|P02747|C1QC_HUMAN	Complement C1q subcomponent subunit C	1.00	10	5	25.3%	**ND Cells - CR**	↑
		19	sp|P01009|A1AT_HUMAN	Alpha-1-antitrypsin	1.00	19	11	40.7%	**ND Cells - CR**	↑

		20	sp|Q15113|PCOC1_HUMAN	Procollagen C-endopeptidase enhancer 1	1.00	23	11	46.5%	**ND Cells - CR**	↑
		21	sp|P03956|MMP1_HUMAN	Interstitial collagenase	1.00	49	17	43.5%	**ND Cells - CR**	↑
		22	sp|P02462-2|CO4A1_HUMAN	Collagen alpha-1(IV) chain	1.00	12	7	7.5%	**ND Cells +CR**	↓
	9. Golgi	**1**	sp|O00461|GOLI4_HUMAN	Golgi integral membrane protein 4	1.00	11	8	13.9%	**ND Cells +CR**	↓
		2	sp|Q08379|GOGA2_HUMAN	Golgin subfamily A member 2	1.00	7	5	5.3%	**ND Cells +CR**	↓
		3	sp|O95573|ACSL3_HUMAN	Long-chain-fatty-acid--CoA ligase 3	1.00	26	20	36.8%	0.021	↓
		4	sp|Q9UI14|PRAF1_HUMAN	Prenylated Rab acceptor protein 1	1.00	6	4	22.2	0.022	
	10. Membrane	**1**	sp|Q6V0I7-3|FAT4_HUMAN	Protocadherin Fat 4	1.00	18	17	5.4%	**ND Cells +CR**	↓
		2	sp|Q92629-2|SGCD_HUMAN	Delta-sarcoglycan	1.00	7	6	25.2%	**ND Cells +CR**	↓
		3	sp|Q92542-2|NICA_HUMAN	Nicastrin	1.00	15	7	21.3%	0.021	↓

		4	sp|O60462-2|NRP2_HUMAN	Neuropilin-2	1.00	17	11	15.2%	0.025	↓
	11. Mitochondrion	**1**	sp|P30038|AL4A1_HUMAN	Delta-1-pyrroline-5-carboxylate dehydrogenase, mitochondria	1.00	7	7	23.2%	**ND Cells +CR**	↓
		2	sp|Q9Y3E5|PTH2_HUMAN	Peptidyl-tRNA hydrolase 2, mitochondrial	1.00	7	3	32.4%	**ND Cells +CR**	↓
		3	sp|P42704|LPPRC_HUMAN	Leucine-rich PPR motif-containing protein, mitochondrial	1.00	85	50	42.8%	0.018	↓
		4	sp|P11766|ADHX_HUMAN	Alcohol dehydrogenase class-3	1.00	11	7	34.8%	85.5	↑
	12. Nucleus	**1**	sp|O60502|NCOAT_HUMAN	Bifunctional protein NCOAT	1.00	13	11	17	**ND Cells +CR**	↓
		2	sp|Q9UIA9|XPO7_HUMAN	Exportin-7	1.00	6	6	7.5%	**ND Cells +CR**	↓
		3	sp|O14980|XPO1_HUMAN	Exportin-1	1.00	42	22	28.4%	0.014	↓
		4	sp|Q9HCU0|CD248_HUMAN	Endosialin	1.00	19	13	22.7%	0.017	↓
	13. Organelle	**1**	sp|O00461|GOLI4_HUMAN	Golgi integral membrane protein 4	1.00	11	8	13.9%	**ND Cells +CR**	↓

	lumen	**2**	sp|P46783|RS10_HUMAN	40S ribosomal protein S10	1.00	16	7	47.9%	0.004	↓
		3	sp|O95479|G6PE_HUMAN	GDH/6PGL endoplasmic bifunctional protein	1.00	29	21	37%	0.0129	↓
		4	sp|Q9UBQ7|GRHPR_HUMAN	Glyoxylate reductase/hydroxypyruvate reductase	1.00	8	7	36.3%	**ND Cells - CR**	↑
	14. Proteosome	**N/A**	N/A							
	15. Ribosome	**1**	sp|P98179|RBM3_HUMAN	Putative RNA-binding protein 3	1.00	8	2	19.1%	**ND Cells +CR**	↓
		2	sp|P61513|RL37A_HUMAN	60S ribosomal protein L37a	1.00	8	6	66.3%	**ND Cells +CR**	↓
		3	sp|P62266|RS23_HUMAN	40S ribosomal protein S23	1.00	11	4	29.4%	0.006	↓
		4	sp|P05386|RLA1_HUMAN	60S acidic ribosomal protein P1	1.00	9	3	66.7%	0.014	↓
	16. spliceosomal complex	**1**	sp|P62318|SMD3_HUMAN	Small nuclear ribonucleoprotein Sm D3	1.00	10	3	33.3%	0.009	↓
		2	sp|O75533|SF3B1_HUMAN	Splicing factor 3B subunit 1	1.00	28	16	17.8%	0.011	↓
	17. vacuole		sp|Q01628|IFM3_HUMAN	Interferon-induced transmembrane protein 3	1.00	7	2	36.6	0.003	↓

			sp|Q6IAA8|LTOR1_HUMAN	Ragulator complex protein LAMTOR1	1.00	17	6	50.3%	0.016	↓
Biological Processes	**1. Cell Communication**	**1**	sp|Q14517|FAT1_HUMAN	Protocadherin Fat 1	1.00	17	14	3.9%	**ND Cells +CR**	↓
		2	sp|P50552|VASP_HUMAN	Vasodilator-stimulated phosphoprotein	1.00	7	4	12.4%	**ND Cells +CR**	↓
		3	sp|P19784|CSK22_HUMAN	Casein kinase II subunit alpha'	1.00	6	5	21.1%	**ND Cells - CR**	↑
		4	sp|P29323-2|EPHB2_HUMAN	Ephrin type-B receptor 2	1.00	7	9	13.4%	**ND Cells - CR**	↑
	2. Cell Death	**1**	sp|Q9Y3E5|PTH2_HUMAN	Peptidyl-tRNA hydrolase 2, mitochondrial	1.00	7	3	32.4%	**ND Cells +CR**	↓
		2	sp|P49588|SYAC_HUMAN	Alanine--tRNA ligase, cytoplasmic	1.00	33	24	33.3%	0.007	↓
		3	sp|Q14974|IMB1_HUMAN	Importin subunit beta-1	1.00	75	33	51.3%	0.019	↓
		4	sp|P00738|HPT_HUMAN	Haptoglobin	1.00	8	10	39.5%	**ND Cells - CR**	↑
	3. Cell Differentiation	**1**	sp|Q99426|TBCB_HUMAN	Tubulin-folding cofactor B	1.00	9	8	44.3%	**ND Cells +CR**	↓
		2	sp|Q9HB71|CYBP_HUMAN	Calcyclin-binding protein	1.00	7	6	52.4%	**ND Cells +CR**	↓

		3	sp|Q86YZ3|HORN_HUMAN	Hornerin	1.00	21	11	20.2%	**ND Cells - CR**	↑
		4	sp|P20930|FILA_HUMAN	Filaggrin	1.00	50	26	16.2%	**ND Cells - CR**	↑
	4. Cell Division	**1**	sp|Q8TD19|NEK9_HUMAN	Serine/threonine-protein kinase Nek9	1.00	6	6	8.7%	**ND Cells +CR**	↓
	5. Cell Growth	**1**	sp|Q9Y2X3|NOP58_HUMAN	Nucleolar protein 58	1.00	12	9	22.7%	**ND Cells +CR**	↓
		2	sp|Q6IAA8|LTOR1_HUMAN	Ragulator complex protein LAMTOR1	1.00	17	6	50.3%	0.016	↓
		3	sp|Q7L576|CYFP1_HUMAN	Cytoplasmic FMR1-interacting protein 1	1.00	30	24	21.6%	0.016	↓
	6. Cell Organisation and Biogenesis	**1**	sp|Q92629-2|SGCD_HUMAN	Delta-sarcoglycan	1.00	7	6	25.2%	**ND Cells +CR**	↓
		2	sp|Q9Y3A5|SBDS_HUMAN	Ribosome maturation protein SBDS	1.00	7	5	32.8%	**ND Cells +CR**	↓
		3	sp|Q9UBQ7|GRHPR_HUMAN	Glyoxylate reductase/hydroxypyruvate reductase	1.00	8	7	36.3%	**ND Cells - CR**	↑
		4	sp|P03956|MMP1_HUMAN	Interstitial collagenase	1.00	49	17	43.5%	**ND Cells - CR**	↑
	7. Cell	**1**	sp|P68036|UB2L3	Ubiquitin-conjugating	1,00	10	6	61.5%	**ND Cells**	↓

	Proliferation		_HUMAN	enzyme E2 L3					**+CR**	
		2	sp|P27487|DPP4_HUMAN	Dipeptidyl peptidase 4	1.00	6	7	9.5%	**ND Cells +CR**	↓
		3	sp|Q13616|CUL1_HUMAN	Cullin-1	1.00	6	6	8.6%	0.023	↓
		4	sp|P35354|PGH2_HUMAN	Prostaglandin G/H synthase 2	1.00	7	7	15.4%	**ND Cells - CR**	↑
	8. Cellular component movement	**1**	sp|Q14517|FAT1_HUMAN	Protocadherin Fat 1	1.00	17	14	3.9%	**ND Cells +CR**	↓
		2	sp|P29317|EPHA2_HUMAN	Ephrin type-A receptor 2	1.00	11	11	13.6%	0.012	↓
		3	sp|P19022|CADH2_HUMAN	Cadherin-2	1.00	24	11	20.8%	0.023	↓
		4	sp|P04114|APOB_HUMAN	Apolipoprotein B-100	1.00	1000	170	47.5%	1393	↑
	9. Cellular homeostasis	**1**	sp|O60502|NCOAT_HUMAN	Bifunctional protein NCOAT	1.00	13	11	17	**ND Cells +CR**	↓
		2	sp|P08237|K6PF_HUMAN	6-phosphofructokinase, muscle type	1.00	8	11	20%	**ND Cells +CR**	↓
		3	sp|P19022|CADH2_HUMAN	Cadherin-2	1.00	24	11	20.8%	0.023	↓

		4	sp|P00738|HPT_HUMAN	Haptoglobin	1.00	8	10	39.5%	**ND Cells - CR**	↑
	10. Coagulation	**1**	sp|P04114|APOB_HUMAN	Apolipoprotein B-100	1.00	1000	170	47.5%	1393	↑
		2	sp|P01009|A1AT_HUMAN	Alpha-1-antitrypsin	1.00	19	11	40.7%	**ND Cells - CR**	↑
		3	sp|P03956|MMP1_HUMAN	Interstitial collagenase	1.00	49	17	43.5%	**ND Cells - CR**	↑
	11. Conjugation	N/A	N/A							
	12. Defense Response	**1**	sp|P09429|HMGB1_HUMAN	High mobility group protein B1	1.00	10	8	35.3%	**ND Cells +CR**	↓
		2	sp|P01859|IGHG2_HUMAN	Ig gamma-2 chain C region	1.00	11	9	41.7%	48.2	↑
		4	sp|P01860|IGHG3_HUMAN	Ig gamma-3 chain C region	1.00	8	10	34.7%	**ND Cells - CR**	↑
		5	sp|P02747|C1QC_HUMAN	Complement C1q subcomponent subunit C	1.00	10	5	25.3%	**ND Cells - CR**	↑
	13. Development	**1**	sp|Q9Y2A7-2|NCKP1_HUMAN	Nck-associated protein 1	1.00	23	17	18.1%	0.006	↓
		2	sp|P23142|FBLN1	Fibulin-1	1.00	10	12	26.3%	0.014	↓

			_HUMAN							
		3	sp|P01024|CO3_HUMAN	Complement C3	1.00	48	29	27.6	1554	↑
		4	sp|Q86YZ3|HORN_HUMAN	Hornerin	1.00	21	11	20.2%	**ND Cells - CR**	↑
		5	sp|Q15113|PCOC1_HUMAN	Procollagen C-endopeptidase enhancer 1	1.00	23	11	46.5%	**ND Cells - CR**	↑
	14. Metabolic Process	**1**	sp|P21810|PGS1_HUMAN	Biglycan	1.00	7	7	28.3%	**ND Cells +CR**	↓
		2	sp|Q13618-2|CUL3_HUMAN	Cullin-3	1.00	8	8	11.2%	**ND Cells +CR**	↓
		3	sp|P04003|C4BPA_HUMAN	C4b-binding protein alpha chain	1.00	9	7	16.9%	**ND Cells - CR**	↑
		4	sp|Q9UBQ7|GRHPR_HUMAN	Glyoxylate reductase/hydroxypyruvate reductase	1.00	8	7	36.3%	**ND Cells - CR**	↑
	15. Regulation of biological process	**1**	sp|P02808|STAT_HUMAN	Statherin	1.00	8	2	54.8%	**ND Cells +CR**	↓
		2	sp|Q9Y3P9|RBGP1_HUMAN	Rab GTPase-activating protein 1	1.00	7	6	6.2%	**ND Cells +CR**	↓
		3	sp|P01009|A1AT_HUMAN	Alpha-1-antitrypsin	1.00	19	11	40.7%	**ND Cells - CR**	↑

		4	sp|P03956|MMP1_HUMAN	Interstitial collagenase	1.00	49	17	43.5%	**ND Cells - CR**	↑
	16. Reproduction	**1**	sp|P61513|RL37A_HUMAN	60S ribosomal protein L37a	1.00	8	6	66.3%	**ND Cells +CR**	↓
		2	sp|P62854|RS26_HUMAN	40S ribosomal protein S26	1.00	7	3	33.9%	0.003	↓
		3	sp|P04114|APOB_HUMAN	Apolipoprotein B-100	1.00	1000	170	47.5%	1393	↑
		4	sp|P35354|PGH2_HUMAN	Prostaglandin G/H synthase 2	1.00	7	7	15.4%	**ND Cells - CR**	↑
	17. Response to Stimulus	**1**	sp|Q9UHA4|LTOR3_HUMAN	Ragulator complex protein LAMTOR3	1.00	8	5	62.1%	**ND Cells +CR**	↓
		2	sp|P52630|STAT2_HUMAN	Signal transducer and activator of transcription 2	1.00	12	10	16.1%	0.003	↓
		3	sp|P01876|IGHA1_HUMAN	Ig alpha-1 chain C region	1.00	21	11	52.4%	395	↑
		4	sp|P01024|CO3_HUMAN	Complement C3	1.00	48	29	27.6	1554	↑
		5	sp|P02747|C1QC_HUMAN	Complement C1q subcomponent subunit C	1.00	10	5	25.3%	**ND Cells - CR**	↑
	18.	**1**	sp|Q9H223|EHD4	EH domain-containing	1.00	6	9	17.6%	**ND Cells**	↓

	Transport		_HUMAN	protein 4					**+CR**	
		2	sp|Q9UIA9|XPO7_HUMAN	Exportin-7	1.00	6	6	7.5%	**ND Cells +CR**	↓
		3	sp|P51571|SSRD_HUMAN	Translocon-associated protein subunit delta	1.00	20	6	37%	0.026	↓
		4	sp|P04114|APOB_HUMAN	Apolipoprotein B-100	1.00	1000	170	47.5%	1393	↑

Table S2b: Media proteomics analysis with CR (+CR) and without CR (-CR); (↑) indicates upregulation, whilst (↓) indicates down regulation; ND indicates Not Detected.

			Protein Accession No	Description	Inter Prophet Probability	Peptide Spectrum Matches (PSMs)	Unique peptides	% Coverage	SINQ Media+CR / Media-CR	(↑) / (↓)
Molecular Functions	**1. Antioxidant activity**	**1**	sp|P10620|MGST1_HUMAN	Microsomal glutathione S-transferase 1	1.000	14	5	30.3%	ND +CR	↓
	2. Catalytic activity	**1**	sp|P67812|SC11A_HUMAN	Signal peptidase complex catalytic subunit SEC11A	1.000	6	6	38.7%	ND +CR	↓
		2	sp|O75390|CISY_HUMAN	Citrate synthase	1.000	7	6	14.8%	0.006	↓
		3	sp|Q08188|TGM3_HUMAN	Transglutaminase-3	1.000	13	7	14.1%	58.955	↑
		4	sp|P20930|FILA_HUMAN	Filaggrin	1.000	13	7	1.2%	87.670	↑
	3. DNA binding	**1**	sp|P23396|RS3_HUMAN	40S ribosomal protein S3	1.000	13	7	32.5%	ND +CR	↓
		2	sp|P10809|CH60_HUMAN	60 KDa heat shock protein, mitochondrial	1.000	9	6	15.9%	ND + CR	↓
	4. Enzyme	**1**	sp|P46940|IQGA1	Ras GTPase-activating-like	1.000	8	8	6.7%	ND +CR	↓

	regulator activity		_HUMAN	protein IQGAP1						
		2	sp|P10619|PPGB_HUMAN	Lysosomal protective protein	1.000	7	3	6.7%	ND +CR	↓
		3	sp|Q03135|CAV1_HUMAN	Caveolin-1	1.000	27	10	62.4%	0.002	↓
		4	tr|Q3SYB4|Q3SYB4_HUMAN	Serpin B12	1.000	16	9	25.6%	245.327	↑
	5. Metal ion binding	**1**	sp|P51571|SSRD_HUMAN	Translocon-associated protein subunit delta	1.000	13	5	36.4%	ND +CR	↓
		2	sp|P02792|FRIL_HUMAN	Ferritin light chain	1.000	13	5	41.1%	ND +CR	↓
	6. Motor activity	**1.**	sp|Q14204|DYHC1_HUMAN	Cytoplasmic dynein 1 heavy chain 1	1.000	7	8	2.4%	ND +CR	↓
	7. Nucleotide Binding	**1**	sp|P61019|RAB2A_HUMAN	Ras-related protein Rab-2A	1.000	12	9	56.1	ND +CR	↓
		2	sp|P61106|RAB14_HUMAN	Ras-related protein Rab-14	1.000	10	9	52.6%	ND +CR	↓
		3	sp|Q9NP72|RAB18_HUMAN	Ras-related protein Rab-18/RAB18	1.000	6	6	35.9%	ND +CR	↓
		4	sp|P14625|ENPL_HUMAN	Endoplasmin	1.000	44	30	42.1%	0.003	↓
	8. Protein binding	**1**	sp|Q9NQC3-2|RTN4_HUMA	Reticulon-4	1.000	9	6	22.9%	ND +CR	↓

			N							
		2	sp|P10915|HPLN1_HUMAN	Hyaluronan and proteoglycan link protein 1	1.000	6	5	18.6%	ND +CR	↓
		3	sp|P24821-4|TENA_HUMAN	Tenascin/Tenascin-C	1.000	47	41	27.9%	0.002	↓
		4	sp|P12111|CO6A3_HUMAN	Collagen alpha-3(VI) chain	1.000	327	131	51.4%	0.004	↓
		5	sp|Q15149|PLEC_HUMAN	Plectin	1.000	157	138	34.2%	0.005	↓
		6	sp|P02679-2|FIBG_HUMAN	Fibrinogen gamma chain	1.000	7	2	6.4%	ND -CR	↑
		7	sp|Q13835-2|PKP1_HUMAN	Plakophilin-1	1.000	23	19	33.2%	ND -CR	↑
	9. Receptor activity	**1**	sp|P08865|RSSA_HUMAN	40S ribosomal protein SA	1.000	9	7	38.6%	**ND +CR**	↓
		2	sp|P24390|ERD21_HUMAN	ER lumen protein retaining receptor 1	1.000	7	4	26.9%	**ND +CR**	↓
		3	sp|P05556|ITB1_HUMAN	Integrin beta-1/Fibronectin receptor subunit beta	1.000	24	12	17.9%	0.005	↓
		4	sp|Q99623|PHB2_HUMAN	Prohibitin-2	1.000	8	8	32.1%	0.007	↓
	10. RNA	**1**	sp|P23396|RS3_	40S ribosomal protein S3	1.000	13	7	32.5%	**ND +CR**	↓

	binding		HUMAN							
		2	sp|P62081|RS7_HUMAN	40S ribosomal protein S7	1.000	15	8	51%	**ND +CR**	↓
		3	sp|P61978-2|HNRPK_HUMAN	Heterogeneous nuclear ribonucleoprotein K	1.000	7	5	21.6%	**ND +CR**	↓
		4	sp|Q9UBQ5|EIF3K_HUMAN	Eukaryotic translation initiation factor 3 subunit K	1.000	6	4	20.4%	**ND +CR**	↓
	11. Signal transducer activity	**1**	sp|Q9UBI6|GBG12_HUMAN	Guanine nucleotide-binding protein G(I)/G(S)/G(O) subunit gamma-12	1.000	6	5	69.4%	**ND +CR**	↓
	12. Structural Molecule activity	**1**	sp|Q99715|COCA1_HUMAN	Collagen alpha-1(XII) chain	1.000	170	77	33.5%	0.005	↓
		2	sp|Q00610-2|CLH1_HUMAN	Clathrin heavy chain 1	1.000	24	21	21.6%	0.017	↓
		3	sp|Q02383|SEMG2_HUMAN	Semenogelin-2	1.000	9	12	30.4%	**ND -CR**	↑
		4	sp|P04279|SEMG1_HUMAN	Semenogelin-1	1.000	11	13	34%	**ND -CR**	↑
	14. Translation regulator	**1**	sp|P62263|RS14_HUMAN	40S ribosomal protein S14	1.000	10	5	37.7%	**ND +CR**	↓
		2	sp|P46781|RS9_H	40S ribosomal protein S9	1.000	8	7	28.4%	**ND +CR**	↓

	activity		UMAN							
	15. Transporter activity	**1**	sp|P12236|ADT3_HUMAN	ADP/ATP translocase 3	1.000	10	7	31.9%	**ND +CR**	↓
		2	sp|P00403|COX2_HUMAN	Cytochrome c oxidase subunit 2	1.000	6	5	27.8%	**ND +CR**	↓
		3	sp|Q07954|LRP1_HUMAN	Prolow-density lipoprotein receptor-related protein 1	1.000	40	30	7.9%	0.013	↓
		4	sp|Q01469|FABP5_HUMAN	Fatty acid-binding protein, epidermal	1.000	19	11	69.5%	2365.566	↑
Cellular Components	**1 Cell Surface**	**1**	sp|P06576|ATPB_HUMAN	ATP synthase subunit beta	1.000	26	19	58.6%	**ND +CR**	↓
		2	sp|P10809|CH60_HUMAN	60 KDa heat shock protein, mitochondrial	1.000	9	6	15.9%	**ND +CR**	↓
		3	sp|Q03135|CAV1_HUMAN	Caveolin-1	1.000	27	10	62.4%	0.002	↓
		4	sp|P11279|LAMP1_HUMAN	Lysosome-associated membrane glycoprotein 1	1.000	11	6	12.7%	0.002	↓
	3 Cytoplasm	**1**	sp|P63000-2|RAC1_HUMAN	Ras-related C3 botulinum toxin substrate 1	1.000	7	6	29.2%	**ND +CR**	↓
		2	sp|Q9P2E9-2|RRBP1_HUMA	Ribosome-binding protein 1	1.000	17	14	20%	**ND +CR**	↓

			N							
		3	sp|P47929|LEG7_HUMAN	Galectin-7	1.000	11	7	71.3%	**ND -CR**	↑
	4 Cytoskeleton	**1**	sp|P62081|RS7_HUMAN	40S ribosomal protein S7	1.000	15	8	51%	↓	↓
		2	sp|Q14204|DYHC1_HUMAN	Cytoplasmic dynein 1 heavy chain 1	1.000	7	8	2.4%	**ND +CR**	↓
	6 Endoplasmic Reticulum	**1**	sp|P04844-2|RPN2_HUMAN	Dolichyl-diphosphooligosaccharide--protein glycosyltransferase subunit 2	1.000	6	4	14.3%	**ND +CR**	↓
		2	sp|P67812|SC11A_HUMAN	Signal peptidase complex catalytic subunit SEC11A	1.000	6	6	38.7%	**ND +CR**	↓
		3	sp|P30101|PDIA3_HUMAN	Protein disulfide-isomerase A3	1.000	25	19	44.2%	0.002	↓
		4	sp|P14625|ENPL_HUMAN	Endoplasmin	1.000	44	30	42.1%	0.003	↓
		5	sp|Q32P28-3|P3H1_HUMAN	Prolyl 3-hydroxylase 1	1.000	6	5	6.9%	0.009	↓
	7 Endosome	**1**	sp|Q9NVJ2|ARL8B_HUMAN	ADP-ribosylation factor-like protein 8B	1.000	10	7	36.6%	**ND +CR**	↓
		2	sp|P10809|CH60_HUMAN	60 kDa heat shock protein, mitochondrial	1.000	9	6	15.9%	**ND + CR**	↓

		3	sp|Q15836|VAMP3_HUMAN	Vesicle-associated membrane protein 3	1.000	9	4	40%	**ND +CR**	↓
		4	sp|P08962|CD63_HUMAN	CD63 antigen/ Granulophysin	1.000	6	2	9%	**ND +CR**	↓
	8 Extracellular	**1**	sp|P10809|CH60_HUMAN	60 kDa heat shock protein, mitochondrial	1.000	9	6	15.9%	**ND + CR**	↓
		2	sp|P13987|CD59_HUMAN	CD59 glycoprotein	1.000	7	2	22.2%	**ND +CR**	↓
		3	sp|Q969H8|CS010_HUMAN	UPF0556 protein C19orf10	1.000	6	4	27.2%	**ND +CR**	↓
		4	sp|P10915|HPLN1_HUMAN	Hyaluronan and proteoglycan link protein 1	1.000	6	5	18.6%	**ND +CR**	↓
		5	sp|P35442|TSP2_HUMAN	Thrombospondin-2	1.000	16	15	17%	0.002	↓
		6	sp|Q99715|COCA1_HUMAN	Collagen alpha-1(XII) chain	1.000	170	77	33.5%	0.005	↓
		8	sp|P02679-2|FIBG_HUMAN	Fibrinogen gamma chain	1.000	7	2	6.4%	**ND -CR**	↑
		9	sp|P05160|F13B_HUMAN	Coagulation factor XIII B chain	1.000	7	6	14.7%	**ND -CR**	↑
		10	sp|Q02383|SEMG2_HUMAN	Semenogelin-2	1.000	9	12	30.4%	**ND -CR**	↑
		11	sp|P04279|SEMG	Semenogelin-1	1.000	11	13	34%	**ND -CR**	↑

			1_HUMAN							
		12	sp|P36952|SPB5_HUMAN	Serpin B5	1.000	11	10	39.5%	**ND -CR**	↑
		13	sp|P47929|LEG7_HUMAN	Galectin-7	1.000	11	7	71.3%	**ND -CR**	↑
		14	sp|P10809|CH60_HUMAN	60 kDa heat shock protein, mitochondrial	1.000	9	6	15.9%	ND + CR	↓
		15	sp|P13987|CD59_HUMAN	CD59 glycoprotein	1.000	7	2	22.2%	ND +CR	↓
	9 Golgi	**1**	sp|P61019|RAB2A_HUMAN	Ras-related protein Rab-2A	1.000	12	9	56.1	ND +CR	↓
		2	sp|P61106|RAB14_HUMAN	Ras-related protein Rab-14	1.000	10	9	52.6%	ND +CR	↓
		3	sp|P49755|TMEDA_HUMAN	Transmembrane emp24 domain-containing protein 10	1.000	17	8	37.4%	0.002	↓
		4	sp|O75396|SC22B_HUMAN	Vesicle-trafficking protein SEC22b	1.000	24	7	38.1%	0.006	↓
	10 Membrane	**1**	sp|P60903|S10AA_HUMAN	Protein S100-A10	1.000	14	6	48.5%	ND +CR	↓
		2	sp|Q9NQC3-2|RTN4_HUMAN	Reticulon-4	1.000	9	6	22.9%	ND +CR	↓
		3	sp|P49755|TMED	Transmembrane emp24	1.000	17	8	37.4%	0.002	↓

			A_HUMAN	domain-containing protein 10						
	11 Mitochondrion	**1**	sp|Q00325-2|MPCP_HUMAN	Phosphate carrier protein	1.000	10	6	25.2%	ND +CR	↓
		2	sp|O75947-2|ATP5H_HUMAN	ATP synthase subunit d, mitochondrial	1.000	6	6	46.7%	ND +CR	↓
		3	sp|Q99623|PHB2_HUMAN	Prohibitin-2	1.000	8	8	32.1%	0.007	↓
		4	sp|P21796|VDAC1_HUMAN	Voltage-dependent anion-selective channel protein 1/Plasmalemmal porin	1.000	10	7	30.4%	0.012	↓
	12 Nucleus	**1**	sp|P13073|COX41_HUMAN	Cytochrome c oxidase subunit 4 isoform 1	1.000	9	7	41.4%	ND +CR	↓
		2	sp|Q9UBQ5|EIF3K_HUMAN	Eukaryotic translation initiation factor 3 subunit K	1.000	6	4	20.4%	ND +CR	↓
		3	sp|Q9NP72|RAB18_HUMAN	Ras-related protein Rab-18/RAB18	1.000	6	6	35.9%	ND +CR	↓
		4	sp|Q99623|PHB2_HUMAN	Prohibitin-2	1.000	8	8	32.1%	0.007	↓
	15 Ribosome	**1**	sp|P23396|RS3_HUMAN	40S ribosomal protein S3	1.000	13	7	32.5%	ND +CR	↓

		2	sp|P62280|RS11_HUMAN	40S ribosomal protein S11	1.000	14	8	50.6%	ND +CR	↓
		3	sp|Q02543|RL18A_HUMAN	60S ribosomal protein L18a	1.000	8	6	35.2%	ND +CR	↓
		4	sp|P30050|RL12_HUMAN	60S ribosomal protein L12	1.000	10	6	54.4%	0.004	↓
	17 vacuole	**1**	sp|Q9NVJ2|ARL8B_HUMAN	ADP-ribosylation factor-like protein 8B	1.000	10	7	36.6%	ND +CR	↓
		2	sp|P61106|RAB14_HUMAN	Ras-related protein Rab-14	1.000	10	9	52.6%	ND +CR	↓
		3	sp|P11279|LAMP1_HUMAN	Lysosome-associated membrane glycoprotein 1	1.000	11	6	12.7%	0.002	↓
		4	sp|Q8NBS9|TXND5_HUMAN	Thioredoxin domain-containing protein 5	1.000	11	8	28.1%	0.014	↓
Biological Processes	**1 Cell Communication**	**1**	sp|O60565|GREM1_HUMAN	Gremlin-1	1.000	13	5	35.9%	ND +CR	↓
		2	sp|P62820|RAB1A_HUMAN	Ras-related protein Rab-1A	1.000	7	9	53.7%	ND +CR	↓
		3	sp|P05556|ITB1_HUMAN	Integrin beta-1/Fibronectin receptor subunit beta	1.000	24	12	17.9%	0.005	↓
		4	sp|P21796|VDAC1_HUMAN	Voltage-dependent anion-selective channel protein 1/Plasmalemmal porin	1.000	10	7	30.4%	0.012	↓

	2 Cell Death	**1**	sp|P02792|FRIL_HUMAN	Ferritin light chain	1.000	13	5	41.1%	ND +CR	↓
		2	sp|P10809|CH60_HUMAN	60 kDa heat shock protein	1.000	9	6	15.9%	ND + CR	↓
		3	sp|P11279|LAMP1_HUMAN	Lysosome-associated membrane glycoprotein 1	1.000	11	6	12.7%	0.002	↓
		4	sp|P47929|LEG7_HUMAN	Galectin-7	1.000	11	7	71.3%	ND -CR	↑
	3 Cell Differentiation	**1**	sp|P12236|ADT3_HUMAN	ADP/ATP translocase 3	1.000	10	7	31.9%	ND +CR	↓
		2	sp|Q9NQC3-2|RTN4_HUMAN	Reticulon-4	1.000	9	6	22.9%	ND +CR	↓
		3	sp|Q08188|TGM3_HUMAN	Protein-glutamine gamma-glutamyltransferase E/Transglutaminase-3	1.000	13	7	14.1%	58.955	↑
		4	sp|P20930|FILA_HUMAN	Filaggrin	1.000	13	7	1.2%	87.670	↑
	4 Cell Division	**1**	sp|Q9NVJ2|ARL8B_HUMAN	ADP-ribosylation factor-like protein 8B	1.000	10	7	36.6%	ND +CR	↓
	5 Cell Growth	**1**	sp|Q9NQC3-2|RTN4_HUMAN	Reticulon-4	1.000	9	6	22.9%	ND +CR	↓

		2	sp|P62263|RS14_HUMAN	40S ribosomal protein S14	1.000	10	5	37.7%	ND +CR	↓
	6 Cell Organisation and Biogenesis	**1**	sp|Q15836|VAMP3_HUMAN	Vesicle-associated membrane protein 3	1.000	9	4	40%	ND +CR	↓
		2	sp|Q99715|COCA1_HUMAN	Collagen alpha-1(XII) chain	1.000	170	77	33.5%	0.005	↓
		3	sp|Q07954|LRP1_HUMAN	Prolow-density lipoprotein receptor-related protein 1	1.000	40	30	7.9%	0.013	↓
		4	sp|Q8NBS9|TXND5_HUMAN	Thioredoxin domain-containing protein 5	1.000	11	8	28.1%	0.014	↓
	7 Cell Proliferation	**1**	sp|P25705|ATPA_HUMAN	ATP synthase subunit alpha	1.000	33	14	33.6%	ND +CR	↓
		2	sp|P10809|CH60_HUMAN	60 kDa heat shock protein	1.000	9	6	15.9%	ND + CR	↓
		3	sp|P46781|RS9_HUMAN	40S ribosomal protein S9	1.000	8	7	28.4%	ND +CR	↓
		4	sp|P36952|SPB5_HUMAN	Serpin B5	1.000	11	10	39.5%	ND -CR	↑
	8 cellular component movement	**1**	sp|P06576|ATPB_HUMAN	ATP synthase subunit beta	1.000	26	19	58.6%	ND +CR	↓
		2	sp|Q14204|DYHC1_HUMAN	Cytoplasmic dynein 1 heavy chain 1	1.000	7	8	2.4%	ND +CR	↓
		3	sp|Q03135|CAV1	Caveolin-1	1.000	27	10	62.4%	0.002	↓

			_HUMAN							
	9 cellular homeostasis	**1**	sp|P06576|ATPB_HUMAN	ATP synthase subunit beta	1.000	26	19	58.6%	ND +CR	↓
		2	sp|P14625|ENPL_HUMAN	Endoplasmin	1.000	44	30	42.1%	0.003	↓
		3	sp|Q8NBS9|TXND5_HUMAN	Thioredoxin domain-containing protein 5	1.000	11	8	28.1%	0.014	↓
	10 Coaguation	**1**	sp|P08962|CD63_HUMAN	CD63 antigen/ Granulophysin	1.000	6	2	9%	ND +CR	↓
		2	sp|Q03135|CAV1_HUMAN	Caveolin-1	1.000	27	10	62.4%	0.002	↓
		3	sp|P02679-2|FIBG_HUMAN	Fibrinogen gamma chain	1.000	7	2	6.4%	ND -CR	↑
		4	sp|P05160|F13B_HUMAN	Coagulation factor XIII B chain	1.000	7	6	14.7%	ND -CR	↑
	12 Defense Response	**1**	sp|P39656|OST48_HUMAN	Dolichyl-diphosphooligosaccharide--protein glycosyltransferase 48 kDa subunit	1.000	19	15	53.5%	ND +CR	↓
		2	sp|P12236|ADT3_HUMAN	ADP/ATP translocase 3	1.000	10	7	31.9%	ND +CR	↓
		3	sp|P14625|ENPL_HUMAN	Endoplasmin	1.000	44	30	42.1%	0.003	↓

	13 Development	**1**	sp|P00403|COX2_HUMAN	Cytochrome c oxidase subunit 2	1.000	6	5	27.8%	ND +CR	↓
		2	sp|Q9UBI6|GBG12_HUMAN	Guanine nucleotide-binding protein G(I)/G(S)/G(O) subunit gamma-12	1.000	6	5	69.4%	ND +CR	↓
		3	sp|P20930|FILA_HUMAN	Filaggrin	1.000	13	7	1.2%	87.670	↑
		4	sp|Q01469|FABP5_HUMAN	Fatty acid-binding protein, epidermal	1.000	19	11	69.5%	2365.566	↑
	14 Metabolic Process	**1**	sp|P30044-2|PRDX5_HUMAN	Peroxiredoxin-5	1.000	14	8	72.8%	ND +CR	↓
		2	sp|Q9NVJ2|ARL8B_HUMAN	ADP-ribosylation factor-like protein 8B	1.000	10	7	36.6%	ND +CR	↓
		3	sp|Q08188|TGM3_HUMAN	Protein-glutamine gamma-glutamyltransferase E/Transglutaminase-3	1.000	13	7	14.1%	58.955	↑
		4	sp|P36952|SPB5_HUMAN	Serpin B5	1.000	11	10	39.5%	ND -CR	↑
	15 Regulation of biological process	**1**	sp|P46940|IQGA1_HUMAN	Ras GTPase-activating-like protein IQGAP1	1.000	8	8	6.7%	ND +CR	↓
		2	sp|P63000-2|RAC1_HUMA	Ras-related C3 botulinum toxin substrate 1	1.000	7	6	29.2%	ND +CR	↓

			N							
		3	sp|P14625|ENPL_HUMAN	Endoplasmin	1.000	44	30	42.1%	0.003	↓
		4	sp|P05556|ITB1_HUMAN	Integrin beta-1/Fibronectin receptor subunit beta	1.000	24	12	17.9%	0.005	↓
	16 Reproduction	**1**	sp|P10620|MGST1_HUMAN	Microsomal glutathione S-transferase 1	1.000	14	5	30.3%	ND +CR	↓
		2	sp|P26373|RL13_HUMAN	60S ribosomal protein L13	1.000	6	2	9.5%	ND +CR	↓
		3	sp|Q03135|CAV1_HUMAN	Caveolin-1	1.000	27	10	62.4%	0.002	↓
		4	sp|P30050|RL12_HUMAN	60S ribosomal protein L12	1.000	10	6	54.4%	0.004	↓
	17 Response to Stimulus	**1**	sp|P08962|CD63_HUMAN	CD63 antigen/ Granulophysin	1.000	6	2	9%	ND +CR	↓
		2	sp|P21796|VDAC1_HUMAN	Voltage-dependent anion-selective channel protein 1/Plasmalemmal porin	1.000	10	7	30.4%	0.012	↓
		3	sp|P02679-2|FIBG_HUMAN	Fibrinogen gamma chain	1.000	7	2	6.4%	ND -CR	↑
	18 Transport	**1**	sp|P51571|SSRD_HUMAN	Translocon-associated protein subunit delta	1.000	13	5	36.4%	ND +CR	↓
		2	sp|O75396|SC22	Vesicle-trafficking protein	1.000	24	7	38.1%	0.006	↓

			B_HUMAN	SEC22b						
		3	sp|P21796|VDAC1_HUMAN	Voltage-dependent anion-selective channel protein 1/Plasmalemmal porin	1.000	10	7	30.4%	0.012	↓
		4	sp|Q00610-2|CLH1_HUMAN	Clathrin heavy chain 1	1.000	24	21	21.6%	0.017	↓